LABORATORI NAZIONALI DI FRASCATI
SIS – Pubblicazioni

LNF–01/027(IR)
12 Novembre 2001

RAP Proposal

RAP collaboration

S. Bertolucci[1], M. Cirillo[2], E. Coccia[2], A. de Waard[3], D. Di Gioacchino[1], V. Fafone[1], G. Frossati[3], A. J. Lobo[4], A. Marini[1], G. Mazzitelli[1], V. Merlo[2], I. Modena[2], G. Modestino[1], L. Pellegrino[1], G. Pizzella[5], L. Quintieri[1], G. Raffone[1], F. Ronga[1], R. Russo[2], P. Tripodi[6], P. Valente[1]

[1]INFN Laboratori Nazionali di Frascati
[2]INFN Sezione di Roma 2 and Dipartimento di Fisica, Università di Roma "Tor Vergata"
[3]Kamerlingh Onnes Laboratory, Leiden University, The Netherlands
[4]Departament de Física Fonamental, Universitat de Barcelona, Spain
[5]INFN Laboratori Nazionali di Frascati and Dipartimento di Fisica, Università di Roma "Tor Vergata"
[6]INFN Laboratori Nazionali di Frascati and ENEA Centro Ricerche Frascati

Contents

1 Introduction

The resonant-mass gravitational wave (GW) detector NAUTILUS, an aluminum 2300 kg cylinder cooled at 100 mK [1], has recently recorded signals due to the passage of cosmic rays [2].

In 1969 Beron and Hofstander had already carried out experiments aiming to detect oscillations of piezoelectric disks excited by a GeV electron beam. The results led the authors to suggest that a very large cosmic-ray (CR) event could excite mechanical vibrations in a metallic cylinder at its resonance frequency and could provide an accidental background for experiments on GW's [3, 4]. Later, a group at the University of Milan [5] estimated the possible effects of particles on a small aluminum cylinder and made an experiment which verified the calculations, although with rather large experimental errors.

The mechanical vibrations originate from the local thermal expansion caused by warming up due to the energy lost by the particles crossing the material. The effect depends on the thermal expansion coefficient and the specific heat of the material. The ratio of these two quantities is the Grüneisen coefficient. It turns out that while both the expansion coefficient and the specific heat vary with temperature, the Grüneisen coefficient practically does not. In the case of aluminum, this is certainly true above 1 K, but no data are available at lower temperatures when the aluminum becomes superconductor.

Subsequently, more refined calculations were made by several authors [6]-[10]. All these models agree in predicting, for the vibrational energy E of the excited fundamental mode of an aluminium cylindrical bar like NAUTILUS, the following formula:

$$E = 7.64 \cdot 10^{-9} W^2 f \tag{1}$$

where E is expressed in kelvin, W, in GeV, is the energy released by the particle to the bar and f is a geometrical factor of the order of unity. The above formula has recently been verified with an experiment at room temperature [11], using a small aluminium cylinder and an electron beam.

NAUTILUS has been operating in continuous data taking at the INFN Frascati Laboratory for three years. The measured strain sensitivity at the two resonances is $3 \cdot 10^{-22}$ Hz$^{-1/2}$ over a bandwidth of 0.5 Hz, corresponding to a noise temperature T_{eff} of about 2 mK, with a duty cycle only limited by cryogenic operations.

NAUTILUS is equipped with a CR detector [12]. The data regarding the vibrational energy of the bar have been correlated with the data obtained by the CR detector. Very large signals, at a rate much greater than expected have been detected [13].

In order to investigate this matter and account for these anomalous re-

sults we propose to measure the effect of the passage of charged particles in a low temperature mechanical oscillator in a controlled environment. We plan to use the DAΦNE electron Beam Test Facility (BTF) at LNF to excite mechanical vibrations in a small cylindrical bar made of the same aluminum alloy as NAUTILUS. The measurements will be performed in both superconducting and normal regime of the aluminum bar.

Moreover, the measurement will be done using energies of the order of 1 TeV. This is the typical energy released in the bar by the extensive air showers producing the "anomalous signals". It means an improvement in sensibility of about 10^4 - 10^5 with respect to past experiments.

In section 2 we describe the main concepts of the thermo-acoustic model and give a summary of the experiments performed up to now to study the excitation of mechanical vibrations in metallic bodies impinged by elementary particles. In section 3 we summarize the results obtained with the CR's in the NAUTILUS detector. In section 4 we briefly review the physics of the interaction of radiation and ionizing particles with superconducting materials in the form of bulk or thin films, covering the aspects that, in our present opinion, could be relevant for the development of the RAP project, and we examine a recently proposed effect (charge effect) associated with the passage of CR's through a bar detector. In section 5 we describe the experimental set-up and in the last section the costs and the schedule of the proposed experiment.

The results of this experiment will be important to understand the interactions of ionizing particles with bulk superconductors and also to understand the limitations due to CR's to the sensitivity of the future gravitational resonant detectors not shielded against CR's.

The proponents are grateful to D. Babusci, M. Bassan and G. Giordano, for their contributions to this proposal.

2 The thermo-acoustic detection of particles in gravitational wave detectors. Experimental facts.

2.1 Introduction

The production of mechanical vibrations in solid or liquid materials by elementary particles has been widely considered for many applications.

As an example, in the case of liquid absorbers, sound detection has been proposed for shower calorimetry or muon identification in massive deep underwater telescopes, mainly dedicated to neutrino astronomy. In ref. [14], which also summarizes the theoretic and experimental knowledge in this field, results of experiments performed at BNL and Harvard University are reported, demonstrating that a detectable signal is produced by energetic proton beams in traversing a liquid medium and that the observed acoustic signal is consistent with the prediction of the thermal expansion model.

In this section, however, attention is focused on the results obtained in the detection of mechanical vibrations in metallic bodies impinged by elementary particles, and, in particular, in the experiments that motivated this research with the argument that the generated vibrations could in principle limit the sensitivity of GW resonant detectors exposed to CR's. All the experiments reported were conducted at room temperature.

2.2 The thermo-acoustic model

The underlying model for the acoustic detection of high energy particles is based on the assumption that the energy released by a particle traversing a material gives rise to local heating and thus to a mechanical tension leading to a pressure pulse. Various authors [4]-[9] have evaluated the effect due to the passage of particles in a metallic bar. The following is the estimate given in [10] for the vibrational energy, E, in the $n-th$ longitudinal mode of a metallic cylinder:

$$E = (4k/9\pi)(\gamma^2/\rho L v^2)(dW/dx)^2 F_n(z_0, \theta_0, l_0) \tag{2}$$

with:

$$F_n(z_0, \theta_0, l_0) = \left[\sin\left(\frac{n\pi z_0}{L}\right) \frac{\sin \frac{n\pi l_0 cos\theta_0}{2L}}{\frac{n\pi R cos\theta_0}{L}}\right]^2 \tag{3}$$

where in (2) k is the Boltzmann constant, ρ the density of the material, L the length of the bar, v the sound velocity in the material, dW/dx the energy loss of the particle in the material and γ the adimensional Grüneisen parameter:

$$\gamma = \frac{\alpha K_T V}{C_V} \tag{4}$$

containing the material thermal expansivity, α, the isothermal bulk modulus, K_T, the constant-volume heat capacity, C_V; γ is considered constant with temperature and for aluminum this is true above $T \approx 1$K, but no data are available at lower values of temperature, where the material behaves as a superconductor.The track and the absorber geometric properties are factorised in (3) and, in particular, R is the radius of the bar and z_0, θ_0, l_0 are, respectively, the distance of the track midpoint from one end of the bar, the angle of the track with respect to the axis of the bar and the length of the track in the bar; the fundamental mode is considered when (3) is applied to the RAP case.

2.3 The experiments

Beron, B.L. and Hoftstadter, R., in their pioneering work [3], reported on the observation of radial and compressional modes of vibration of a set of piezoelectric disks impinged by electron beams of 0.2-1.0 GeV energy. The authors also explicitly mentioned that a very large CR event could excite mechanical vibrations in a metallic cylinder at its resonant frequencies and could provide an accidental background for experiments on GW's.

Grassi Strini, A.M. et al. [5] deemed the results obtained in the Beron and Hoftstadter experiment not exhaustive due to the fact that a set-up with no calibration capacities was used, that the interpretation of the results was merely qualitative and that the observations could have been affected by the energy spread in the absorber caused by the showering electrons. In the Grassi Strini et al. experiment a cylindrical bar, 20 cm in length and 3 cm in diameter, made of an aluminum alloy and suspended in a vacuum chamber by a steel wire, was used. Two piezoelectric transducers, one placed in correspondence to the central cross section of the bar and the other displaced with respect to that section, provided the readout of the oscillations, also enabling even harmonics detection. The whole system was calibrated by exciting the bar with an oscillating electrical force. The bar was exposed either to a 29.3 MeV pulsed proton beam with a peak intensity of 5 μA and time duration ranging from 10 to 50 μs or to a 500 eV pulsed electron beam with currents of several mA and time duration between 10 and 50 μs. The maximum oscillation amplitude of the first, second and third harmonic as a function of the energy delivered in the beams was the experimental observable, with a quoted total error of $\pm 20\%$. Comparison with the predictions of a simplified model was performed (assuming that: (1) all the beam energy is transformed into thermal energy, (2) the bar can be described as a unidimensional elastic system, (3) the energy of the beam spreads out uniformly on the whole cross section of the bar, (4) the beam pulse duration is short with respect to the oscillation period of the highest order harmonics). The agreement was very satisfactory in the case of the proton beam.

The less satisfactory agreement found for the electron beams was referred to the limitations of the theoretical model adopted, and in particular to the unfulfilment of the third hypothesis, since the electron energy was too low to allow for penetration inside the bar material, leaving the localisation of the electron energy loss in the regions near the surface and, thus, not allowing the use of a unidimensional model (second hypothesis) as a good approximation.

Verification of the thermo-acoustic model, as described in [5], was also attempted by Bressi G., et al. [15] using a suspended cylindrical test mass, length 20 cm and diameter 3 cm, made of an aluminum alloy with an innovative transducer [16] detecting the change of the tunneling current when there is a variation of the gap between a tip and the surface of the macroscopic body to be monitored. Various calibrated set-up were exposed to proton beams in order to detect the effect. The first attempt was made at LNL with a 5 MeV proton beam with a negative observational result, which was ascribed to unfulfilment of the third hypothesis in the above indicated model, since the range of a 5 MeV proton is 0.18 mm. The second attempt was made at the LNL Tandem by using a proton beam of 30 MeV energy, in order to insure the uniformity of the energy release in the bar, being 4 mm the proton range at this energy. The negative observational result was related to the time duration of the proton pulse, not optimally matching the fourth hypothesis of the model. The last attempt was made at CERN using LEAR, delivering 50 MeV protons with pulse time duration shorter than LNL Tandem; this set-up was subject to a irrecoverable environmental seismic noise, with effect also in the tunneling current, and electrical induction on the sensors. The dismission of LEAR made improvement of the experimental conditions impossible.

A recent experiment [11] has confirmed the applicability of the model by using different set-up exposed to a ≈ 600 MeV electron beam operating in single bunch mode with a pulse width of up $\approx 2\mu$s and adjustable intensity of $10^9 - 10^{10}$ electrons per bunch, provided by the Amsterdam linear accelerator, MEA, now dismissed.
One set-up consisted in a cylindrical bar, made of an aluminum alloy and of 20 cm length and 3.5 cm diameter. The bar was suspended by a plastic string connected to a horizontally movable gliding structure, allowing for displacement of the bar with respect to the beam spot, inside a vacuum chamber. Different arrangements of sensors and calibrators were used in order to verify the feasibility and then to perform the measurement. In the latter case a piezoelectric sensor was placed 1 cm off center on top of the bar; one end of the bar was equipped with an accelerometer, the other end facing a capacitor plate. The calibration of the piezoelectric sensor was performed against the accelerometer, by using the excitation provided by a loudspeaker, and the stability of the piezoelectric device was monitored

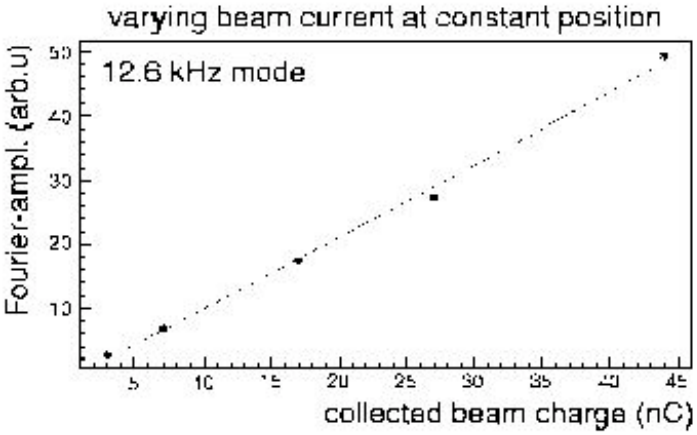

Figure 1: *Correlation between the Fourier amplitude of the 12.6 kHz vibrational mode and the beam charge. Data points(*) and straight line fit(-). - From ref.([11])*

during the runs by electrically driving the capacitor plate.
Calculations using the thermo-acoustic model agreed well with the data, as demonstrated by the variations of the excitation strength with the absorbed energy, inferred from the linear dependence between the Fourier amplitude of the modes on the integrated charge in the beam pulse at a fixed beam position (Fig.1), and by comparison of the amplitudes with the model predictions as a function of the beam hit positions along the cylinder. A conversion factor of 7.4± 1.4 nm/J was found for the first longitudinal mode of the resonator, while the prediction of the model is 10 nm/J.

3 Summary of the Experimental Data with Cosmic Rays in NAUTILUS

3.1 Introduction

In this section we summarize the results of the CR's obtained by the ROG collaboration with the NAUTILUS antenna, published in [2, 13]. A discussion of possible sources of the large amplitude events is reported. We also anticipate results obtained by the ROG group with a NAUTILUS run at non superconductor temperature suggesting that at least the large events are correlated to the temperature.

3.2 NAUTILUS data : normal low amplitude events

NAUTILUS is equipped with a CR detector system consisting of seven layers of streamer tubes for a total of 116 counters [12]. Three superimposed layers, each with an area of 36 m^2, are located over the cryostat. Four superimposed layers are under the cryostat, each one with area of 16.5 m^2. Each counter measures the charge, which is proportional to the number of particles. The detector is able to measure particle density up to $5000\frac{\text{particles}}{\text{m}^2}$ without large saturation effects. and it gives a rate of showers in good agreement with the expected number [12, 17], as verified using the particle density in the streamer tubes over the cryostat (up particle density), which is not affected by the interaction in the NAUTILUS detector.

The rate of events due to CR in the NAUTILUS antenna was calculated using GEANT to simulate NAUTILUS and the CORSIKA [18] Montecarlo to simulate the effect of the hadrons produced by the CR interactions in the atmosphere. The results are in table 1.

Since the expected signal amplitude is quite small in the first [2] search for signals due to CR's, analysis using a zero threshold method was performed, that is, a search adding the NAUTILUS data streams with a time offset given from the CR events (selected with a cut on the particle density bigger than 600 particles/m^2). The conclusion of this work was that the amplitude of the detected signal was in rough agreement with the calculations (within a factor 3).

Table 1: Calculated events/day due to cosmic rays.

Energy(K)	Muons	Ext Air Showers	Hadrons	Total
10^{-5}	12.7	50	24.2	87
10^{-4}	1.2	7	3	11.2
10^{-3}	0.18	0.8	0.33	1.3
10^{-2}	0.002	0.1	0.05	0.15

Later on a few events having very large amplitude in the NAUTILUS

antenna were found, so a search of coincidences started.

3.3 NAUTILUS data : large amplitude events

Using the same data as in [2], coincidences between the NAUTILUS events and the signals from the CR NAUTILUS detectors were searched, for a total observation time of 83.4 days [13]. As result of this analysis a clear coincidence excess above background is found, when the showers have particle density large enough to give a signal in the bar. There are 18 coincidences for the down particle density greater than 300 $\frac{\text{particles}}{\text{m}^2}$, while the expected number of accidentals is $n = 2.1$ For a particle density greater than 600 $\frac{\text{particles}}{\text{m}^2}$ the coincidences reduce to twelve, with n = 0.78.

An unexpected, extremely large NAUTILUS event in coincidence with a CR event, with energy $E = 57.89$ Kelvin was found, corresponding to 87 TeV released in the bar. Both the up and down particle density of the CR detector are the largest in this case. The time of the NAUTILUS event is obtained with good accuracy from the data, given the very large value of SNR=15860: $t_o = 2123.928$ s with an error of the order of 10 ms. The time when the event is observed is 2123.9222 s with a time error better than 1 ms. The difference of 6 ms is within the experimental error of the G.W. time events (at present time accuracy for the NAUTILUS apparatus has been improved). The good agreement between the two times excludes the possibility that the large amplitude signals are due to electrical noise on the SQUID.

The 57.89 Kelvin value should be compared to the value obtained using the down particle density under the hypothesis of electromagnetic showers. In the previous work [2], finalized to the study of small signals, it was found that this energy is given by $E = \Lambda^2\ 4.7\ 10^{-10}$ Kelvin where Λ is the number of particles in the bar. For the biggest event the above equation gives $E =$ 0.019 K, which is more than three orders of magnitude smaller than the recorded 58 K. In the same way energies much smaller than those reported for all the coincident events are obtained. The conclusion is that all or most of the observed NAUTILUS events are not due to electromagnetic showers.

On the contrary, when using the NAUTILUS measurements at zero time delay with energy of the order or below the noise and adding them up at the CR trigger time, as in the previous analysis, it was found that the electromagnetic showers account for the energy observations within a factor of three. For the previous result [2] the energy of the small signals is correlated with the CR particle density. By contrast, no correlation with the lower particle density is found for the 18 large signals. This is shown in fig. 2, and confirms the idea that the observed large events are not due to pure electromagnetic showers. In conclusion, the NAUTILUS signals are associated with two distinct families of CR showers. In one family the signals can be interpreted as due to the electromagnetic component of the showers,

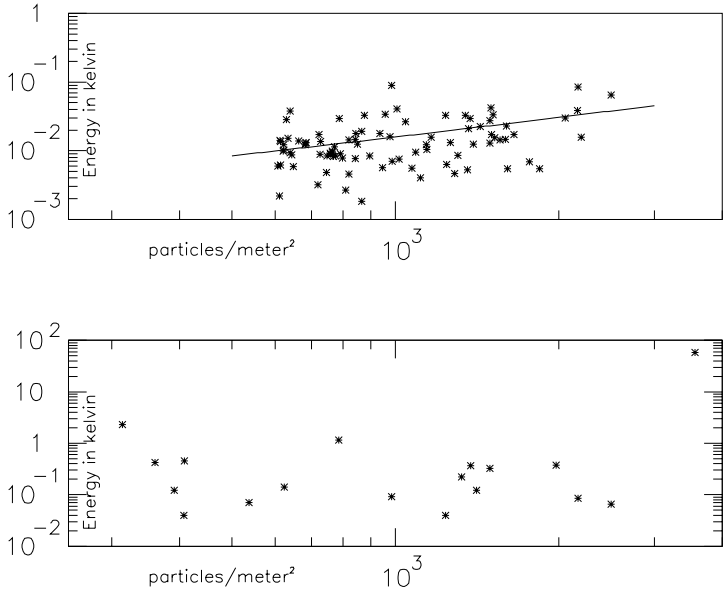

Figure 2: *Correlation between the NAUTILUS signals and cosmic ray particle density. The upper graph shows the correlation of the NAUTILUS energy at zero delay (with respect to the cosmic ray events) versus the corresponding cosmic ray lower particle density, for the 92 data points considered in the previous analysis. The correlation coefficient is 0.30, with a probability of being accidental of less than 1%. Instead, the lower plot shows no correlation between the energy of the NAUTILUS coincident events analysed in this paper and the corresponding cosmic ray particle density (from ref. [13]).*

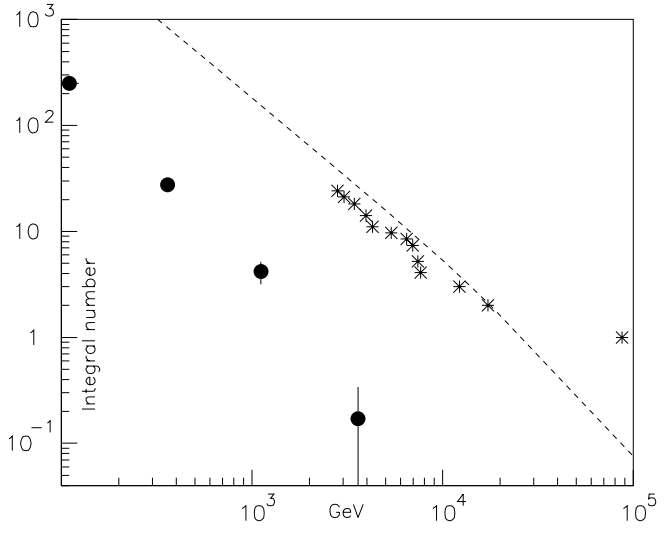

Figure 3: *Comparison between calculations and measurements (from ref. [13]). The asterisks indicate the integrated number of coincident events versus the energy released by the cosmic ray to the bar, expressed in GeV units, to be compared with the points having error bars, which give the number of events due to hadrons we expect in the NAUTILUS bar. The dashed line is the experimental integral spectrum for the hadronic component of the showers, for the 83.4 days of observation, obtained by the Kascade experiment. See text.*

in the other family the known CR particles in the shower do not justify the amplitude or the rate of the observed signals.

One must consider the possibility that the large events are due to the contribution of hadrons in the showers. The rates calculated in table 1 appear to disagree with the observation by more than one order of magnitude. In figure 3 the calculated numbers are compared with the integrated number of coincidences versus the NAUTILUS event energy. Using eq. (1) it is possible to express the integral number in terms of the energy released to the NAUTILUS bar by the CR's.

In this figure there are also recent measurements [19] of the hadronic components of extensive air showers, the number of hadronic showers versus their total energy measured with usual particle detectors. Comparison of these measurements with the result of the Monte Carlo calculation shown in fig. 3 with the error bars proves that the calculations have been performed correctly, since, because of the small diameter of the bar, only a few percent of the hadronic energy should be absorbed by the bar, just as shown in fig. 3.

An immediate finding is that the highest energy event occurs in a time

Table 2: Coincidences Cosmic Rays - NAUTILUS.

Data	Temp. (K)	Days	Events	Accidentals	Rate (ev./day)
Sept-Dec 1998	0.1	83.4	18	2	0.19 ± 0.051
Feb-Jul 2000	0.1	31.8	13	2.3	0.33 ± 0.11
Total T=0.1 K	0.1	115.2	31	4.3	0.23 ± 0.048
Aug 00 Aug 01	1.1	65.7	6	3.4	0.04 ± 0.04

period more than one hundred times shorter than estimated under the hypothesis that the signals in the bar are due to hadrons. This big specific event could be explained as due to a large fluctuation, but a large disagreement between predicted and observed rates also appears for all other events. Thus our observations exceed expectations by one or two orders of magnitude.

Other possibilities to explain these results must be considered, such as anomalous composition of CR's (the observed showers might include other particles, like nuclearites [8, 20, 21] or Q-balls [22]).

We must also take into account the possibility that formula (1) does not always apply, either because the Grüneisen coefficient might be larger at the temperature of NAUTILUS when the aluminum is superconductor and the specific heat rapidly approaches zero, or because the impact of a particle could trigger non-elastic audiofrequency vibrational modes with a much larger energy release. This has already been suggested [23] for the case of the interaction with GW's, to explain cross-sections possibly higher than calculated. However, in this case the agreement found for the small signals between experiment and calculation using eq. (1) requires that the breaking of the model occur rather infrequently.

The favourite hypothesis is currently the one related to an anomalous behaviour of superconductive aluminum. In fact since August 2000 NAUTLUS has been running at a temperature higher than the critical temperature for aluminum. The result of the coincidence analysis for the overall NAUTILUS data is shown in table 2.

In order to have a direct comparison, the event selection is very similar to the one for the 1998 data (noise temperature less than 10 mKelvin, signal noise ratio bigger than 19.5, particle density greater than $300 \frac{\text{particles}}{\text{m}^2}$) . From this table there is evidence at about 3 σ level that the rate is related to the aluminum temperature. This supports the hypothesis that equation (1) for a fraction of the CR events does not apply to superconductive aluminum. This result is the main motivation for our proposal.

However it must be stressed that the rate probably does not go exactly to 0 for T=1.1 Kelvin as could appear from table 2. Enlarging the data set by applying a very loose noise cut (1 Kelvin) 200 useful days are obtained,

an increase of a factor 3. The results are shown in table 3. At high particle density, a small event excess is found; this result is preliminary because it concerns high noise data.

Table 3: Coincidences cosmic rays - NAUTILUS with non superconductor aluminum and high noise - 200 days.

$\frac{particles}{m^2}$	Events	Accidentals
300	61	63.4
600	25	17.5
1200	13	3.9

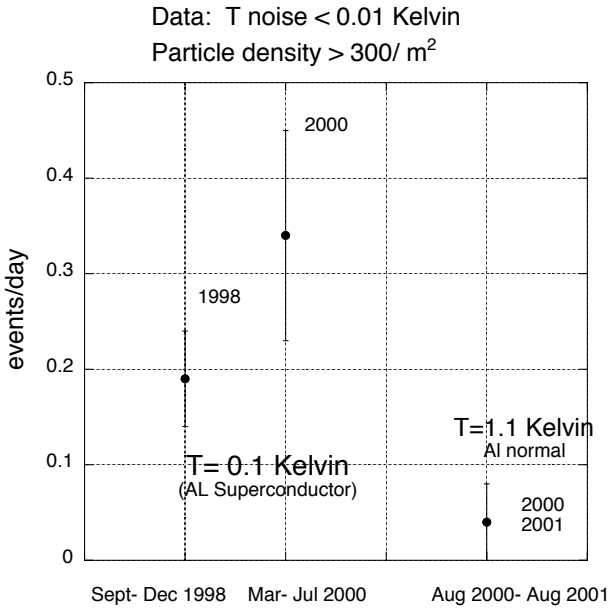

Figure 4: *Rate of events in superconducting and normal aluminum state.*

4 Possible explanations

4.1 Introduction

Among the possible explanations of the observed discrepancy, we can mention some mechanism of mechanical origin in the NAUTILUS bar, such as creep mechanisms or instabilities of plastic deformations at very low temperatures (see sec. 5.2), some unexpected behaviour of NAUTILUS due to its superconducting state (the presence of metastable magnetic domains, or a behaviour of the Grüneisen parameter not taken into account in equation (2)), or some effect of electromagnetic origin, such as the recently proposed "charge effect" or magnetostriction effects. Magnetostriction is present in a ferromagnetic crystal when magnetization induces deformations in the crystal lattice. We do not consider this effect important in our case, because Al5056 is a very weak paramagnetic material, the bar is a polycristal cylinder and the magnetic field produced by the passage of CR's is very low. In the following we will treat in more detail the charge effect, and we will give a brief review of superconducting detectors in order to evidence a possible relevance of superconductivity for the RAP project. Other possibilities to explain our observations could be considered, such as the presence in the shower of exotic particles like nuclearites [20] for instance. Previous searches for these particles with resonant GW detectors have given upper limits [10, 21] not inconsistent with the present experimental data. We note that a resonant GW detector is able to observe particles with a mechanism different from the usual CR detectors.

4.2 Superconductive Detectors

The phenomenon of superconductivity [24] , i. e. the vanishing of electrical resistance and onset of perfect diamagnetism (Meissner effect) below specific critical temperatures and magnetic fields, has for several decades attracted the interest of scientists working in the field of electromagnetic radiation and elementary particles interaction with matter[25, 26]. This attention is generated essentially by the fact that relatively small energy is required in order to break the superconducting groundstate locally. This groundstate is formed by coherent electron pairs (Cooper pairs) whose binding can be destroyed by energies of the order of a few meV. Electromagnetic radiation or ionizing particles releasing such amount of energies to superconductive bulk materials or thin films can perturb the groundstate in a way that can be well detected with room temperature or superconductive electronics.

It is worth recalling here that in 1986 a new family of superconducting materials having transition temperatures above the liquid nitrogen boiling point (77K) was discovered [24] . Although the physics of these new materials having a ceramic (perovskite) structure is surely very stimulating, no reliable microscopic theory explaining the onset of superconductivity in them

has yet appeared. This fundamental lack, along with the poor mechanical properties of the materials, has not generated much radiation and particles detection interest for systems based on this new type of superconductors. For the remainder of these notes we will always consider low temperature superconductors, namely superconductors whose temperature is below 25 K: the structure of these materials is metallic in most of the cases.

Several energy transfer concepts depending on the specific particles or radiation to be detected have been analyzed; however, the peculiarity of all systems and detectors proposed so far is represented by the higher sensitivity of superconductive detectors. Along with the above described low threshold for the breaking of Cooper pairs, the fact that the superconductive systems are operated at temperatures below 10K (in several cases even in the mK region) surely improves sensitivity due to the limited amount of thermal noise. The low thermal noise, however, is not necessarily related to specific physical effects enhancing detector sensitivity.

In the next section we review experiments and processes that represent useful conceptual schemes for the future interpretation of the data to be produced by the RAP experiment. Here, however, we should point out that none of the experiments that we shall be reporting contained a low frequency detection scheme similar to that of the NAUTILUS GW antenna.

4.2.1 Superconductive Detection Schemes

- **Superheating-supercooling detectors**

  This scheme of detection was based on the superheating and supercooling properties of microspheres and granules (diameters from a few tens up to a few hundred microns) of type I superconductors embedded in dielectric materials. The samples, biased by an external magnetic field in the metastable superheating-supercooling region, were supposed to undergo a transition from superconducting to normal state as a result of the interaction with particles and radiation. The materials used were typically indium and tin, and for these materials it was estimated that the system could produce evidence of the interaction even with very weakly interacting particles such as solar neutrinos. The detection system exhibited encouraging sensitivities down to low β and γ sources (the latter down in the keV range) and remarkable sensitivity was reached for the readout electronics up to the point that the switchings of individual granules could be recorded. The practical usefulness of the detection scheme was limited by severe technological problems such as the uniformity of the size of the spheres or granules (along with their large scale production). Nevertheless, we note that this experiment produced evidence of superconducting-normal transitions of microgranules of type I superconductors having radii down to 10μm.

- **The superconducting bolometers**

  A bolometer consists of an absorber and a thermometer in contact with the absorber. When a particle hits the absorber the released energy creates phonons and heat increase. If the heat capacitance of the absorber is low, a condition that can be met at low temperatures, the temperature variations can be measured by the corresponding variations of the thermometric parameters. We note that the absorber itself can also be used as a thermometer. Several systems have been suggested in which the absorber is also made of a superconductor; other typical absorber materials are pure silicon, sapphire or diamond given their low thermal capacity and high diffusivity. Instead, as sensitive thermometers, semiconductor thermistors, superconducting films or superconducting tunnel junctions are used. The basic difference between superconducting and semiconducting absorbers is simply the fact that the process of phonon creation is slightly different in the two cases : for the superconductors, indeed, the deposited energies can also release extra phonons due to electron pairs breaking. The development of bolometers combining semiconducting absorbers and superconductive thermometers is currently a field of intense research and development. These studies have generated, for example, powerful tools in solid state physics in the field of phonon propagation.

- **The tunnel junctions**

  Superconductive tunneling, beside representing an extremely interesting and active research field in condensed matter, has generated a countless number of devices based on SIN (Superconducting-Insulating-Normal), SIS (SuperconductorInsulatingSuperconductor) and Josephson junctions. Tunnel junctions represent the core of superconducting electronics; these have been proposed as ultra-fast descriminators, as thermometers for bolometers, like high-sensitivity direct particle detectors. SIS mixers, Josephson junctions arrays and SQUIDs today represent the best known results of the achievements in superconducting electronics, a field in which several quantum-limited electronic devices have been fabricated.

  The junctions might take advantage of two basic working points on their current-voltage characteristics : the zero-voltage Josephson current and the gap discontinuity. The energy gap discontinuity is generated by the absence of electron tunneling for voltages below the energy gap of superconductors. The discontinuity is accompanied by a very abrupt discontinuity in the current-voltage characteristics, which can be used as a bias point for the detection (particles and radiation) processes. The Josephson current is generated by Cooper pairs when the tunneling barrier is thin enough to allow maintaining the coherence

of the pair itself. The Josephson current can be modulated by weak external magnetic fields, a phenomenon which can give rise to fast switching processes and quantum-limited magnetic field detection.

- **The strip detectors**

  The thin film strip detectors attracted noticeable attention in the last decade when some groups proposed their use in the framework of the SSC (Superconducting Super Collider) project, as basic building block for minimum ionizing particles detectors and 1μm resolution spatial discriminators. The principle of operation of a strip detector is based on the fact that ionizing particles and radiation can locally destroy superconductivity in very thin films (width of the order of 1μm or below). This Cooper pairs breaking generates a pulse because of the abrupt change of resistivity of the film and the pulse, in turn, can be recorded with room temperature electronics. Several experiments were performed on the strip detectors and, in principle their potentiality was demonstrated. However, very little data exist in the literature concerning the most important part of the principle of operation: the self-recovering pulses. The "hot-spots" generated by the incoming particles must be self-recovering : when the pulse has been transmitted the strip must become superconductive again, otherwise the whole principle of the detector is worthless because the "hot-spots" propagate along the strip giving rise to extended normal regions. Although the strip detector represents the simplest device for radiation and particles detections, it has not, since the SSC collider project ended, received much attention.

4.2.2 Possible relevance of superconductivity for the RAP project

Although the experimental evidence indicates that superconductivity of the NAUTILUS bar could be a possible reason for the observation of the anomalous signals recorded at low frequencies, it is not easy at the moment to furnish a consistent and complete explanation. One thing that we tried to make clear in the previous section is the fact that the difference between a normal state and a superconducting state is the condensation of electrons in the form of Cooper pairs. The breaking of these pairs by the energies coming from magnetic fields and temperature gradients represents the characteristic common to all superconducting detectors. Thus, since no difference exists in the crystal structure between a normal metal and a superconductor, any possible explanation must be attributed to an electronic process in which the lattice acts only as an energy transfer vehicle.

The fact that the energy gap of aluminum is of the order of 1 meV shows that that lattice phonons in the submillimeter and infrared region of the spectrum can be excited by Cooper pairs breaking. The propagation

and the mutual interaction of these excitations in a polycrystalline material represents an important point for future speculation. We believe that conclusive data from the NAUTILUS detector (both above and below the critical transition temperature of the aluminum bar) and well focused measurement runs on the bar of the RAP experiment will help clarify the reasons for the anomalous events recorded in coincidence with CR's showers.

4.3 Charge effects

Very recently, R.F. O'Connell has suggested [27] the existence of charge effects associated with the passage of cosmic rays through a bar detector. The analysis of this author is based upon the independent-oscillator (IO) model developed by Ford et al. [28]. This is a very general dissipative *microscopic* model founded on a well defined Hamiltonian, and that leads to an equation of motion in the form of a generalized quantum Langevin equation (GLE).

This equation is usually met in the solution of many dissipative problems arising in various areas of physics (an example being GW detection). For a quantum particle of mass m, the GLE assumes the following form:

$$m\ddot{x} + \int_{-\infty}^{t} \mathrm{d}\tau\, \mu(t-\tau)\, \dot{x}(\tau) + \mathrm{d}V/\mathrm{d}x \;=\; F(t) + f(t)\;, \tag{5}$$

where $\mu(t)$ is the so called memory function, $F(t)$ is the random (fluctuation or noise) force, $f(t)$ is a deterministic external force (e.g., due to a GW) [1], and $V(x)$ a generic external potential. It has been pointed out [28] that the GLE corresponds to a description of a quantum system interacting with a quantum-mechanical heat bath. In fact, in the IO model the system is assumed to be described by the following Hamiltonian:

$$H \;=\; \frac{p^2}{2m} \;+\; V(x) \;-\; xf(t) \;+\; \sum_j \frac{p_j^2}{2m_j} + \frac{1}{2}\, m_j\, \omega_j^2\, (q_j - x)^2\;, \tag{6}$$

where x and p are, respectively, the coordinate and momentum operators for the quantum particle, while q_j and p_j are the corresponding operators for the heat bath oscillator j with mass m_j and frequency ω_j.

A bar detector is usually described as an oscillator of mass m (half of the bar mass) and natural frequency ω_0, dipped in an "Ohmic" (the Fourier transform $\tilde{\mu}$ of the memory function is a real function of ω) heat bath at temperature T. Since the detector is sensitive only in a narrow frequency region around ω_0, $\tilde{\mu}(\omega)$ can be assumed to be a constant ($= m\gamma$). It can be shown [27] that under the further assumption of weak coupling ($\gamma \ll \omega_0$),

[1] In Eq. (5) $x(t)$ is a generalized displacement operator, so that, for instance, Δx could represent an electrical voltage.

the mean square displacement of the oscillator due to the heat bath assumes, in the limit $\hbar\omega_0 \ll kT$, the following form [27]

$$< x^2 >= \frac{kT}{m\omega_0^2} = \frac{2kT}{\hbar\omega_0} < x^2 >_Q \ . \tag{7}$$

where $< x^2 >_Q = \hbar/2m\omega_0$ is the well known expression for uncertainty in the position of a free ($\gamma = 0$) oscillator at $T = 0$.

If the detector acquires a stray charge q, then it will interact with the e.m. fields associated with the ambient blackbody radiation. As a consequence of this interaction the function $\tilde{\mu}(\omega)$ will present a strong frequency dependence. In this case the analysis of the problem is complicated by the mass renormalization of QED. As explicitly derived in ref. [27], denoting with M the renormalized, i.e. *physical*, mass of the charge q, we have:

$$\tilde{\mu}(\omega) = \frac{M\tau_q\Omega^2}{\omega^2+\Omega^2}\,\omega\,(\omega - i\Omega) \ , \tag{8}$$

where Ω is a large cut-off frequency and $\tau_q = 2q^2/3Mc^3$. In general, among M, Ω and the *bare* mass m^* of the charge the following relation holds:

$$M = m^* + \tau_q\,\Omega\,M \ ,$$

from which we see that for $\Omega = 1/\tau_q$ we have $m^* = 0$ (the usual choice for the bare mass of the electron in QED), but the choice $\Omega < 1/\tau_q$ would lead to a positive non-zero value for m^*. In that case, for $T = 0$ we obtain [27]

$$< x^2 >_q = \frac{2}{\pi}\,\omega_0\,\tau_q\ < x^2 >_Q\ \ln\frac{M}{m^*\,\omega_0\,\tau_q} \ , \tag{9}$$

with $< x^2 >_Q$ specialized to the case of a quantum oscillator of mass M. This equation shows that the mean-square displacement of a charged oscillator, as a consequence of the interaction with the zero-point oscillations of the radiation field, is very sensitive to the value of m^*.

Let us now consider the RAP detector ($M \sim 25$ kg, $\nu_0 \sim 4.5$ kHz). In that case $(< x^2 >_Q)^{1/2} = 8.6 \times 10^{-19}$ cm (for $T = 0.1$ K this displacement increases by a factor about 1000). By assuming a stray charge of 1 pC we obtain $\omega_0\tau_q \simeq 2. \times 10^{-37}$. But, this very small number appears also in the denominator of the log argument, together with m^* that, if non zero, has at least a very small value. Actually Eq. (9) is logarithmically divergent as $m^* \to 0$, thus leading to a $< x^2 >_q$ much greater than $< x^2 >_Q$. The author of ref. [27] speculates that this divergence could be cured by a non-zero value for m^* (which would have implications for mass renormalization in QED) or by anharmonic terms which will come into play as $< x^2 >$ grows large. He also stress the necessity to implement the calculation including also retardation and relativistic effects.

In summary, the calculations of ref. [27], although still incomplete, suggest a possible origin for the large non-gravitational signals observed with bar detectors and, as a by-product, identify a possible test for determining the bare mass of the electron. In the light of these results, the possibility to investigate the behaviour of a charged detector in a controlled experiment appears very interesting.

5 Experimental set-up

We plan to use for the proposed experiment a cylindrical bar, cut from a bulk made of the same aluminum alloy (Al5056) as NAUTILUS. The dimensions of the resonator are 205 mm in diameter and 585 mm in length; the resonance frequency of the first longitudinal mode is about 4600 Hz.

In the following we describe the cryogenic system for cooling the bar down to 0.1 K, the mechanical filters needed for isolating the detector from external and internal disturbances, the read-out scheme, the main features of the Beam Test Facility (with a Monte Carlo simulation of the interaction of the beam with the bar) and the data acquisition system.

5.1 Cryogenics

The cryogenic system for the RAP experiment follows basic concepts for any experiment aiming to detect weak effects on a harmonic oscillator at low temperatures:

1. No direct contact between cryogenics and detector, except for the weak thermal connections between refrigerator and suspension system, to minimize the acoustic interference.

2. Fast pre-cooling down to liquid-helium temperatures.

The design of the cryostat is largely determined by the choice of the cooling method, the requirement of long-term operation at mK temperatures, and the design of the low-noise suspension system. It must also take into account the assembling of a detector equipped with sensors. Finally, it must allow for an overpressure compatible with the integrity of the sealing of the inner vacuum vessel. The cryostat is provided by the ROG group and will be available at the end of 2001.

The cooling of the bar and the attached apparatus proceeds in two stages: first, pre-cooling to liquid He temperature, and then the final cooling to 100 mK using a ^{3}He$-^4$He dilution refrigerator.

The first stage determines almost entirely the cool-down time. Calculations made [30] show, that the pre-cooling lasts one day. This can be obtained by forcing He gas directly on the surface of the bar and suspension.

When a temperature of 6 K has been reached, the pre-cooling phase ends, the inner space of the cryostat is evacuated, and the He bath is filled with liquid He. From that point on the dilution refrigerator takes over and the final cooling stage is entered. On extrapolating the measured heat leak of the NAUTILUS detector at 100 mK, a cooling power of 100 μW at 100 mK is a safe design value for the dilution refrigerator. Collaboration with Leiden University has been established and costs have been estimated.

5.2 Mechanical suspensions

The main purpose of a mechanical suspension of a detector is to contribute to the reduction of the seismic noise of the surroundings to a level comparable to the sensitivity of the measuring instruments. In ultra-cryogenic detectors, such as RAP, another aim of the mechanical suspension is to provide the thermal link between the test mass and a dilution refrigerator to allow a good heat sink; furthermore, the mechanical suspension should also provide the thermal insulation between the same dilution refrigerator and the top of the cryostat to avoid heat leakages. Conceptually the suspension is a cascade of attenuation stages [31] (mechanical filters), each consisting of a flexible joint connecting and supporting an inertial mass. The aim of the cascade is to assure the requested level of attenuation inside a proper working frequency window. For the purpose of this experiment, an attenuation of about -150 dB at the bar resonant frequency is needed.

Referring to the mechanical design of the suspension, the use of a finite element code is recommended since the usually adopted spring-mass analytical scheme is sometimes misleading (not to say erroneous), even for simple rods, because it does not take into account: a) cross section shear and rotary inertia effects on high order modes [32]; b) coupling between flexible joints and inertial masses; c) reflection and transmission of waves at discontinuities; d) structural damping, and so on. A "massive" finite element model of the whole suspension is advisable in conjunction with experimental tests on single stage models; as an example of this approach a simple comparison between two stage solutions will be reported later.

In the following pages we give a quite complete discussion of the suspensions for a generic gravitational bar detector; we wish, however, to stress that the requirements of the RAP experiment are less critical than those of a GW experiment, and can easily be satisfied.

5.2.1 Design Criteria

Even if the RAP suspension should carry a very light load (say 100 kg), its design may follow some general criteria which are applied to the suspensions of other cryogenic test facilities carrying much heavier loads, as follows:

- **achieve the best "global attenuation" per unit length stage**;
  the "global attenuation" per unit length is the ratio (expressed in dB) between the modulus of the resulting displacement and the modulus of a completely arbitrary perturbing displacement; since the available room for the suspension is limited by the height of the cryostat, the "global attenuation" per unit length (vertical) is the performance index of the single stage of the suspension;
- **prevent the so called "up conversion" perturbing mechanism**;

low frequency perturbations may produce the relative sliding of two surfaces in contact; the rupture and reformation of the "micro-weldings" in the contact zone lead to high frequency noise; therefore welded joints are preferred instead of any sliding contact such as in bolts, pins, wound cables and soforth;

- **avoid stress concentrations and relieve residual stresses**;

  "Hertz type" contacts (as in threads, knife edge supports, wound cables) and sharp fillets are usually the "loci" of the concentration of stresses which can be suddenly released during the life of the apparatus; these stresses are due to the gravity load acting on the structure and their concentration should be avoided in order not to activate the release process which should be very similar to the creep mechanism; welded joints and rounded fillets are recommended; at the same time, any kind of hardening process (such as cold working, surface machining, drilling and so on), as well as the solidification process of the cast, leave residual stresses which, on the contrary, do not depend on the gravity load; these stresses could be suddenly released and a stress relieving heat treatment is recommended; last but not least, welded and brazed joints between dissimilar materials should be avoided since also the different thermal expansion coefficients give residual stresses which can be dramatically enhanced during the cool-down;

- **take into account cryogenic creep**;

  the creep mechanism may be seen as a noise source too [34, 35]; low stress design is a general rule to avoid creep at any temperature; at cryogenic temperatures the creep mechanism is still present in many metals and only at very low temperatures vanishes (as example the OFHC -Oxygen Free Hight Conductivity- copper does not exhibit a steady state creep at the liquid helium temperature only; see fig. 5); therefore the low stress design is mandatory for the upper part of the suspension which provides the thermal insulation between the dilution refrigerator and the top of the cryostat; on the contrary, the lower part of the suspension (usually made of OFHC copper) may be subjected to high stresses since its working temperature is well below the liquid helium temperature; nevertheless a low stress design for the lower part of the suspension should also be recommended both to have the same working stress level[2] in all the suspension and, of course, for the safety point of view; furthermore [33] there are still some unexplained

[2] If the suspension is made of different materials, the same working stress level is gained by the same ratio between the working stress and the yield stress; the ratio is usually expressed in terms of percentage and common values belong to the range from 10% to 20%.

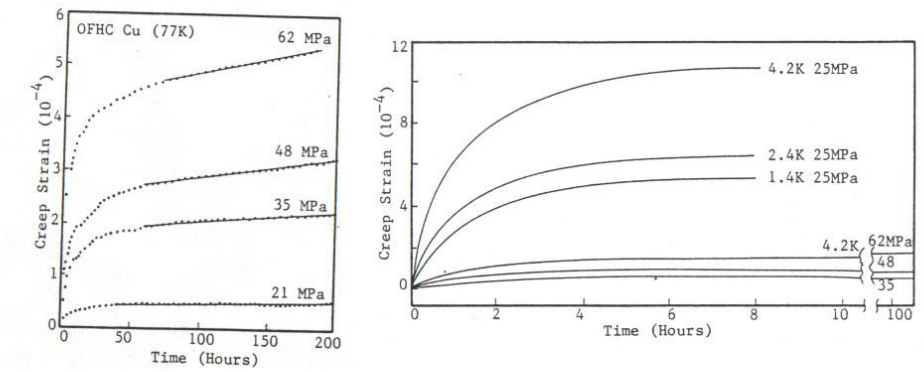

Figure 5: *Creep strain of OFHC copper at nitrogen and liquid helium temperature (from ref.[36]).*

phenomena (as far as the writers know) which develop at very low temperatures, summarized as follows : metal and alloy softening during the superconducting transition (in lead, indium); somewhat strange temperature dependence of the yield stress at very low temperatures (in silver); instability of plastic deformation at very low temperatures (in aluminum and its alloys, see fig. 6); all these items may suggest a low stress approach to the careful designer.

5.2.2 Preliminary design of OFHC copper final stages: tubes and rods suspensions

Due to the light load of the RAP suspension, a good attenuation (in the order of one or two hundreds of dB, as required) can be attained in a small room; as pointed out before, the lower part of the suspension thermally anchors the aluminum cylindrical bar to the refrigerator and must be made of OFHC copper.

OFHC copper is probably the most widely studied cryogenic material; the yield strengths corresponding to the commercially available products are given in table 4; the solutions corresponding respectively to two low design stresses (10 Mpa and 80 Mpa) will be compared[3]; the choice between the

[3]In a completely axially loaded structure high design stresses lead to improved levels of attenuation whatever may be the material.

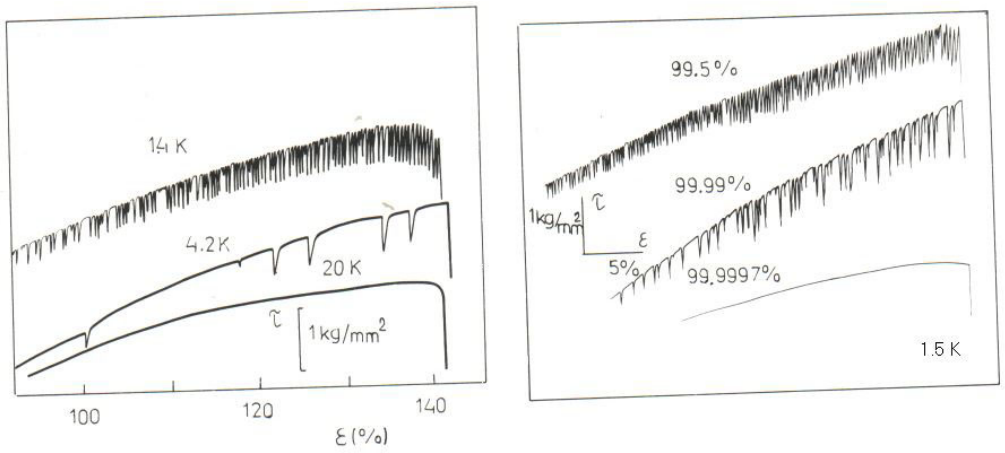

Figure 6: *Effect of the temperature and of the impurity content on the discontinuos behaviour of the plastic deformation in aluminum - stress-strain plots (from ref.[33]).*

Table 4: Design Stress

STATE	YELD STRESS	DESIGN STRESS (20% of yield stress)
annealed	$50 \div 60 MPa$	low working stress: 10 MPa
cold worked	$180 \div 350 MPa$	low working stress: 80 MPa

two design stresses depends mainly on the welding or brazing procedure to be performed and, of course, on the safe margin to be taken into account.

Three values of the inertial mass have been considered (respectively 2, 6 and 10 kg) for a "3 rods" type and a "tube" type suspension; by means of a rough finite element model the single stage "global attenuation" per unit length (vertical) versus the beam length has been obtained and the results are reported in figs. 7 to 10. The attenuation of the stage has been computed for a frequency of 4500 Hz.

It follows that:

1. the "global attenuation" per unit length[4] decreases as the beam length

[4]The "global attenuation" per unit length is defined as the ratio between the attenuation and the beam length increased by 10 mm in order to take into account the room between two consecutive stages.

increases (short beams);

2. the " 3 rods" type curves exhibit more peaks than the "tube" type curves (tuning problem);

3. a "3 rods" solution works better for medium and long beams; for short beams the two solution are more or less the same;

4. increasing the inertial mass usually improves the level of the attenuation.

The high levels of "global attenuation" per unit length obtained for a single stage are somewhat misleading since there can at times be a substantial lowering of this value when more stages are coupled together; for this reason this kind of approach should be repeated for the whole assembled suspension in order to evaluate the real efficiency of the solution[5].

Four design points A, B, C, D have been selected in order to make a preliminary comparison; the points A and B (corresponding to the "3 rods" type) have been taken in the middle of two consecutive peaks; the points C and D (corresponding to the "tube" type) have the same beam length respectively as points A and B; the inertial masses correspond to the best attenuation for the selected lengths (10 kg for A and B, 2 kg for C and 6 kg for D, see table 5).

The design point C is more theoretical rather than practical due to the very thin tube thickness of 0.5 mm; nevertheless for loads much heavier than 100 kg the OFHC copper design stress of 80 Mpa leads to more feasible solutions. Figs. 11 and 12 show the attenuation curves of all the design points and give a preliminary evaluation of the attenuations, windows and so on of the two solutions.

From the above considerations, it appears that the tube suspension might be preferable with respect to the 3 rods solution, even if further investigations are still in progress. In figs.13, 14 a schematic view of the tube suspension is shown.

[5]This approach is computer-time expensive and requires a high degree of detail of the finite element model.

Table 5: Design Point A, B, C, D

	Working Stress: 80 MPa	Working Stress: 10 MPa
" 3 rods type"	DESIGN POINT A inertial mass: 10 Kg rodlength/diameter: 58/2.3 mm attenuation: -45.6 dB attenuation p.u.l: -671.1 dB/m left/right window: 2045/2069 Hz	DESIGN POINT B inertial mass: 10 Kg rodlength/diameter: 93.5/6.5 mm attenuation: -33.4 dB attenuation p.u.l: -322.7 dB/m left/right window: 2055/2086 Hz
"tube type"	DESIGN POINT C inertial mass: 2 Kg tubelength/diameter: 62.5/7.5 mm tube thickness: 0.5 mm attenuation: -44.2 dB attenuation p.u.l: -609.4 dB/m left/right window: 3958/3959 Hz	DESIGN POINT D inertial mass: 6 Kg tubelength/diameter: 83/19 mm tube thickness: 1.5 mm attenuation: -44.4 dB attenuation p.u.l: -477.3 dB/m left/right window: 3768/3711 Hz

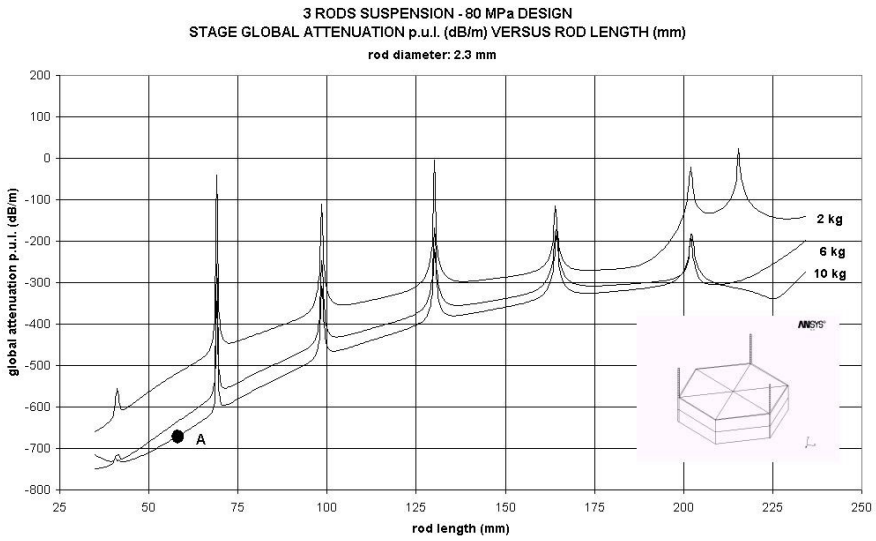

Figure 7: *3 Rods Suspension - 80 MPa design, stage global attenuation p.u.l. (dB/m) versus rod length (mm).*

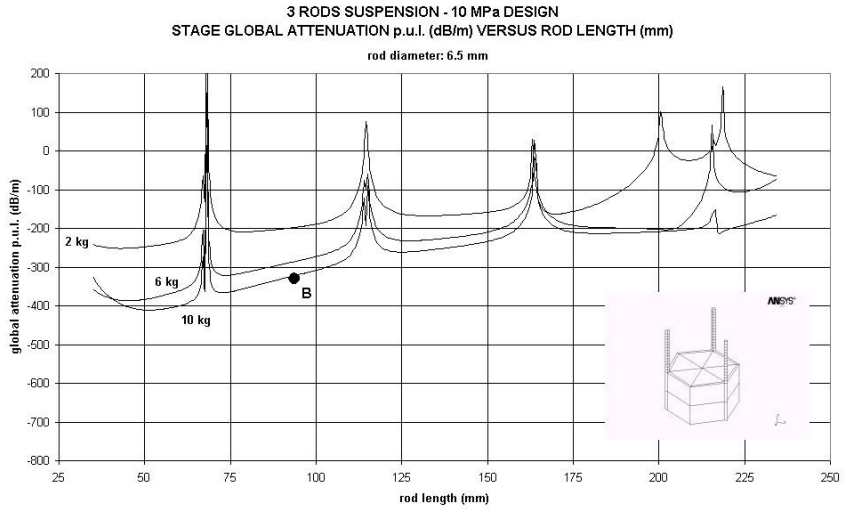

Figure 8: *3 Rods Suspension - 10 MPa design, stage global attenuation p.u.l. (dB/m) versus rod length (mm).*

5.3 Sensitivity and read-out

The mechanical oscillation induced in a resonant-mass detector is transformed into an electrical signal by a motion or strain transducer and then amplified by an electrical amplifier. Inevitably, Brownian motion noise associated with dissipation in the antenna and the transducer, and electronic noise from the amplifier, limit the sensitivity of the detector. Typically, the detector output is filtered with a suitable linear filter designed to optimize the signal-to-noise ratio. We briefly report here the basic notions on the readout systems; for further information see references [37, 38, 39].

The electromechanical transducer can be represented with the components of the Z_{ij} matrix which connects the input variables (force $f(t)$ acting on the transducer and velocity $\dot{x}$(t) of the transducer mechanical parts) with the output variables (voltage $v(t)$ and current $i(t)$):

$$f(t) = Z_{11}\ \dot{x}\ (t) + Z_{12} i(t) \tag{10}$$

$$v(t) = Z_{21}\ \dot{x}\ (t) + Z_{22} i(t) \tag{11}$$

In most common cases the Z_{ij} components satisfy the relationships $Z_{11}Z_{22}$ $= Z_{12}Z_{21}$ and $Z_{12} = Z_{21}$.

An important parameter is the ratio β of the electrical energy in the transducer to the total energy in the resonant body:

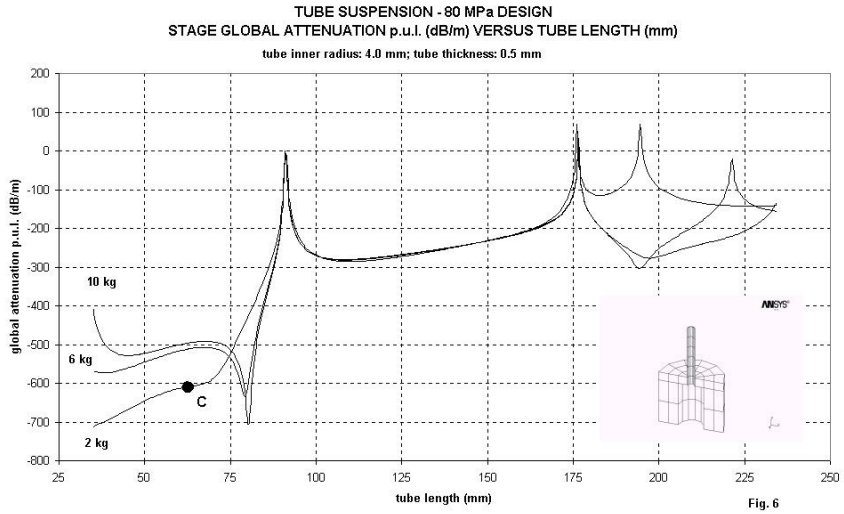

Figure 9: *Tube Suspension - 80 MPa design, stage global attenuation p.u.l. (dB/m) versus rod length (mm).*

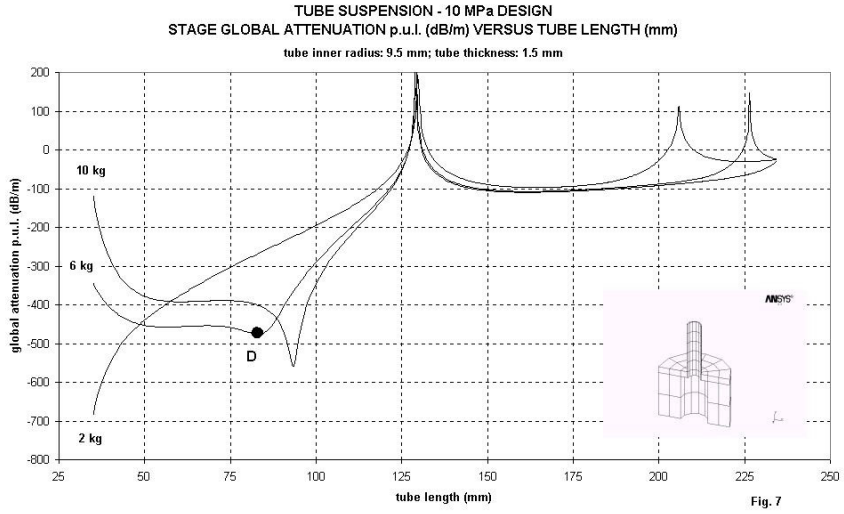

Figure 10: *Tube Suspension - 10 MPa design, stage global attenuation p.u.l. (dB/m) versus rod length (mm).*

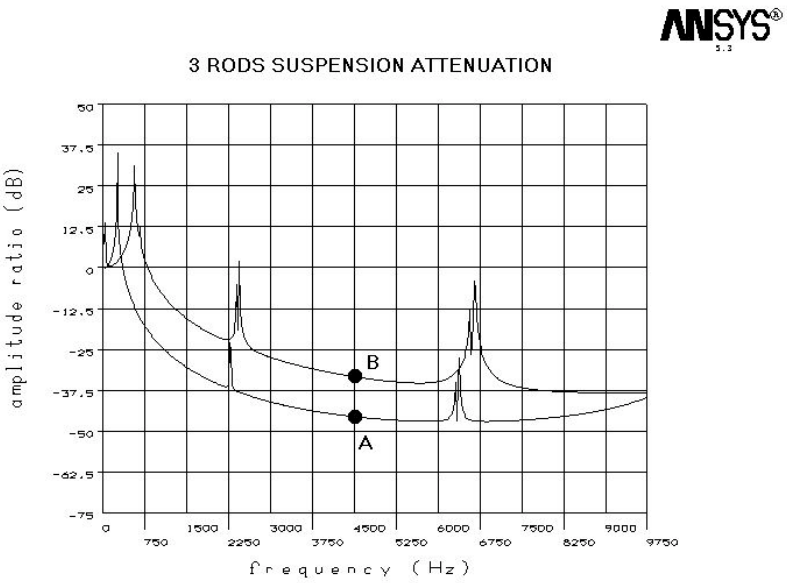

Figure 11: *3 Rods Suspension attenuation.*

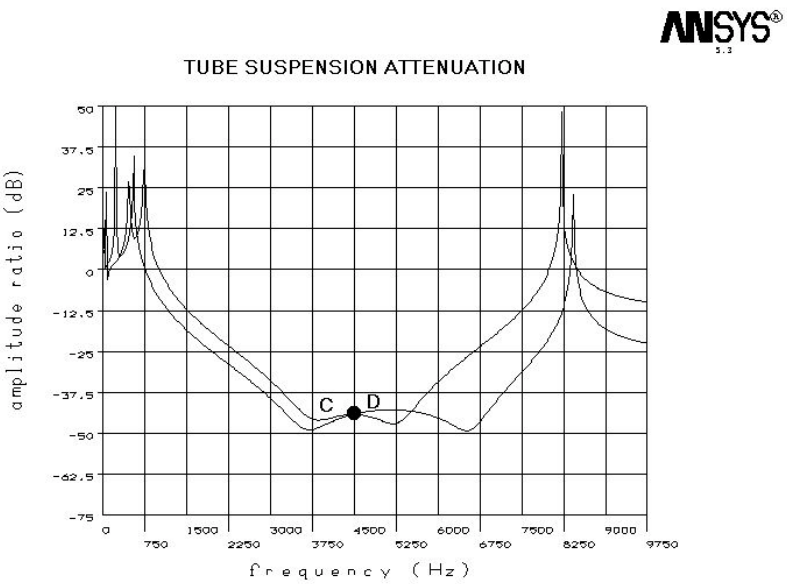

Figure 12: *Tube Suspension attenuation.*

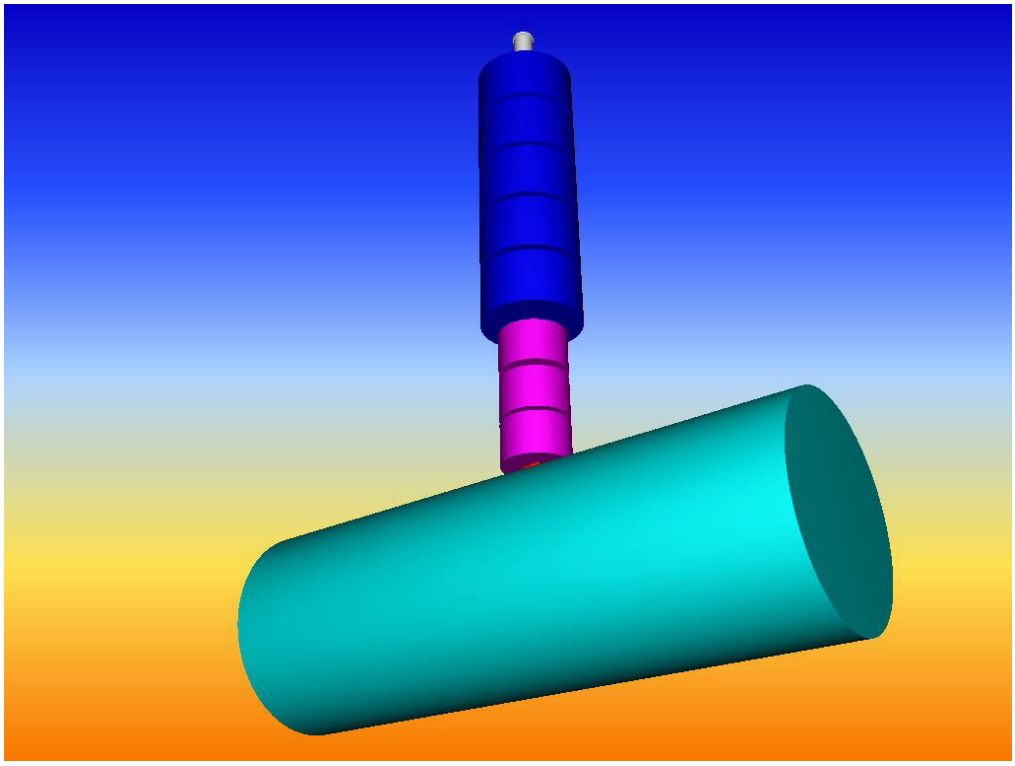

Figure 13: *Schematic view of the tube suspension. The upper five insulation stages are made of stainless steel, in order to provide the proper thermal insulation between the top of the cryostat and the antenna. The three lower stages are made of OFHC copper. Thermal contact with the dilution refrigerator will take place between the stainless steel and the copper stage.*

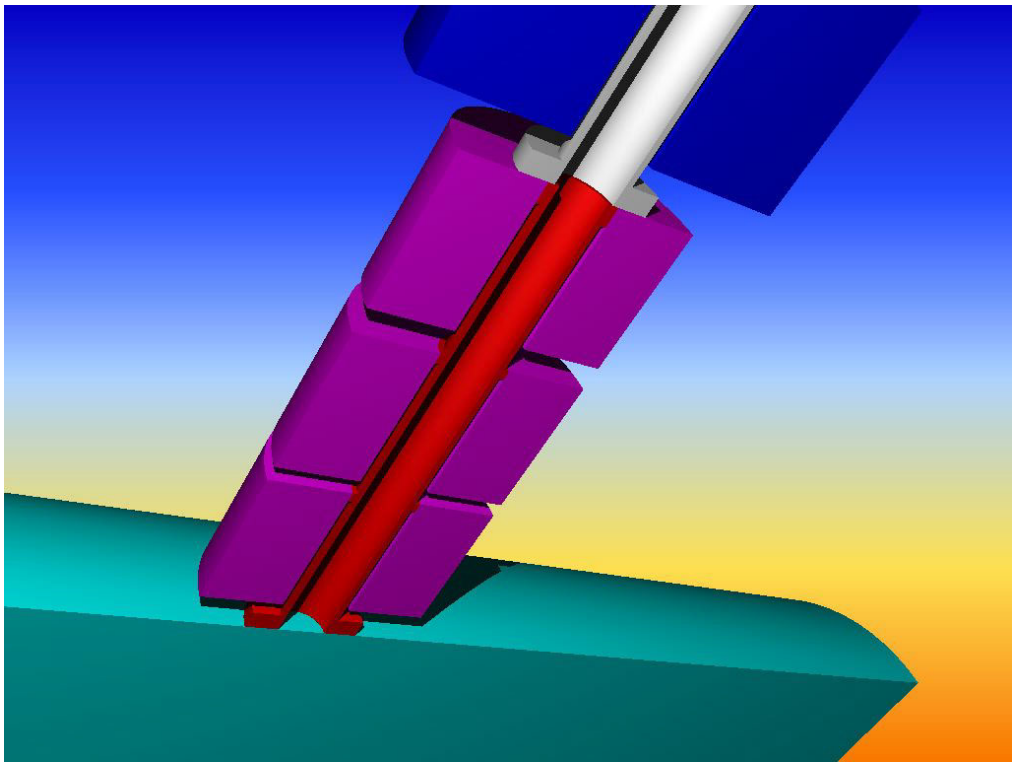

Figure 14: *Section of the tube suspension. The tubes are made of the same material as the surrounding masses.*

$$\beta = \frac{1}{m\omega}\frac{|Z_{21}|^2}{Z_{22}} \tag{12}$$

where m is the effective mass of the monitored mode and ω its angular frequency.

The transducer is connected to an electrical amplifier whose noise can be characterized by two parameters. The two parameters are, usually, the power spectra of the voltage and current noise, V_n^2 and I_n^2, or their following combinations:

$$T_n = \frac{\sqrt{V_n^2 I_n^2}}{K} \tag{13}$$

$$R_n = \sqrt{\frac{V_n^2}{I_n^2}} \tag{14}$$

T_n is called the amplifier noise temperature and R_n the amplifier noise resistance. Another parameter, useful to express the matching between transducer and amplifier, is

$$\lambda = \frac{R_n}{|Z_{22}|} \tag{15}$$

Two classes of noise source have to be considered in the sensitivity analysis of a resonant-mass antenna:

- the intrinsic noise sources such as the thermal and amplifier ones, which have Gaussian statistics and can be accurately characterized, and
- the noise sources such as seismic noise and disturbances from cryogenic liquids, which are more difficult to characterize because they are non-Gaussian and often also non-stationary.

The thermal, or Brownian, noise is due to chaotic motion of the detector atoms in the thermal bath at the temperature T.

The electronic noise has two terms: one is the back action stochastic force exerted by the current noise generator. This acts on the oscillator like the Brownian force.

The effect of the back action noise can be seen as an increment to the oscillator temperature T. The sum of Brownian noise of the oscillator at temperature T and back action noise can be attributed to the Brownian noise of an oscillator with a mechanical quality factor Q at temperature $T_e > T$ where

$$T_e = T\left(1 + \frac{\beta Q T_n}{2\lambda T}\right) \tag{16}$$

The other term is an additive noise due to amplifier and can be considered white in the antenna bandwidth.

Another convenient dimensionless parameter is

$$\Gamma = \frac{T_n(\lambda + 1/\lambda)}{2\beta Q T_e} \tag{17}$$

which gives the ratio of the wide band noise in the resonance bandwidth to the narrow band noise (in practice $\Gamma \ll 1$).

The sum at the output of the contributions given by the Brownian noise (at temperature T_e) and by the wide band electronic noise gives the total detector noise. This can be referred to the input of the detector and is usually indicated as $S_h(f)$:

$$S_h(f) = \frac{1}{\pi^3} \frac{kT_e f_0}{ml^2 Q f^4} \left\{ 1 + \Gamma \left[Q^2 \left(1 - \frac{f^2}{f_0^2} \right)^2 + \frac{f^2}{f_0^2} \right] \right\} \tag{18}$$

where f is the detector resonance frequency, l the effective length and k the Boltzmann constant.

The half height width of this function gives the bandwidth of a resonant detector:

$$\Delta f = \frac{f_0}{Q} \Gamma^{-1/2} \tag{19}$$

This is larger than the pure resonance linewidth f_0/Q.

The problem of extracting a signal of a given shape $h(t)$ from a noise with given spectrum $S_h(f)$ is treated in depth in the information theory.

The optimum performance of a detector is obtained by filtering the output with a filter matched to the signal. The energy signal-to-noise ratio (SNR) of the output of the filter is given by the well known formula

$$SNR = \int_{-\infty}^{+\infty} \frac{|H(f)|^2}{S_h(f)} df \tag{20}$$

where $H(f)$ is the Fourier transform of $h(t)$. Although the integration range is infinite in theory, in practice it will be reduced to the Nyquist band for any specified set of sampled data. For a sampling interval Δt, the Nyquist band is $(-1/2\Delta t, 1/2\Delta t)$. In our case, the passage of a cosmic ray in the bar can be described as an impulsive signal. We model this burst signal as a featureless waveform, rising quickly to an amplitude h_0 and lasting for a time τ_g much shorter then the detector integration time $\Delta t = \Delta f^{-1}$. Its Fourier transform will be considered constant within the detector bandwidth $\Delta f : H(f) \simeq H(f_0) = H_0 \simeq \frac{1}{2} h_0 \tau_g$. From eq. 20 we get:

$$SNR = \frac{\frac{1}{2} m (2\pi f_0)^4 l^2 H_0^2}{4kT_e \sqrt{\Gamma}} \tag{21}$$

The numerator is the energy that the burst would have deposited in the detector mode if it had been initially unexcited. The denominator characterizes the overall noise in the detector and is usually expressed as kT_{eff}; it represents the minimum signal detectable with signal to noise ratio equal to 1. T_{eff} (in Kelvin units) can convenientely be written as

$$T_{eff} = 2T_n \left[\frac{\lambda + \lambda^{-1}}{\lambda} + \frac{2T(\lambda + \lambda^{-1})}{\beta Q T_n} \right]^{1/2} \tag{22}$$

In our experiment we decided to use a read out scheme made with a piezoelectric ceramic (PZT) followed by a FET amplifier, because of its simplicity and in consideration of the goals of the experiment. If we use a commercial PZT ceramic, for which β of the order of 0.3-0.4, and a global mechanical quality factor of 10^3 can be achieved, and a FET amplifier with a voltage noise $V_n \approx 1\text{nV}/\sqrt{\text{Hz}}$ and a current noise $I_n \approx 10^{-15}\text{A}/\sqrt{\text{Hz}}$, values of T_{eff} of the order of 0.3-0.4 K, and a bandwidth of about 0.2 Hz can be achieved for a bar cooled at 0.1 K.

The calibration of the detector equipped with the PZT transducer will be performed by the usual PZT self-calibration technique (applying a known signal to the PZT and detecting it from by the PZT itself [40]). An additional calibration can be performed with a calibrated accelometer.

5.4 Beam characteristics

A Beam Test Facility (BTF) was planned in DAΦNE, the ϕ–factory operating at the Laboratori Nazionali di Frascati of INFN; the main accelerator began operations in 1999, and the BTF will be commissioned in fall 2001 [41, 42].

The BTF is a transfer line starting from the end of the DAΦNE-Linac consisting of by two bending magnets, correctors and four quadrupoles in order to adjust the beam characteristics on the target. The layout of the magnetic elements is shown in fig. 15. The experimental hall (about 100 m^2) is going to be equipped with a multi-head gas system – mostly for particle detector tests – and with cryogenic and water cooling systems. A full data acquisition system, based on VME and NIM standard crates and modules, will also be available for beam-test data taking. A number of signal cables have already been installed from the experimental area to the BTF control room.

The main characteristics of the BTF electron beam are listed in table 6. Even if the maximum Linac energy is 800 MeV, when working in parasitic mode to the main DAΦNE experiments the beam energy is 510 MeV. We will refer to this operating mode in the following. An example of the optical function, calculated with the MAD code, is shown in fig. 16: a wide range of beam spot size can easily be spanned to match the experimental requirements.

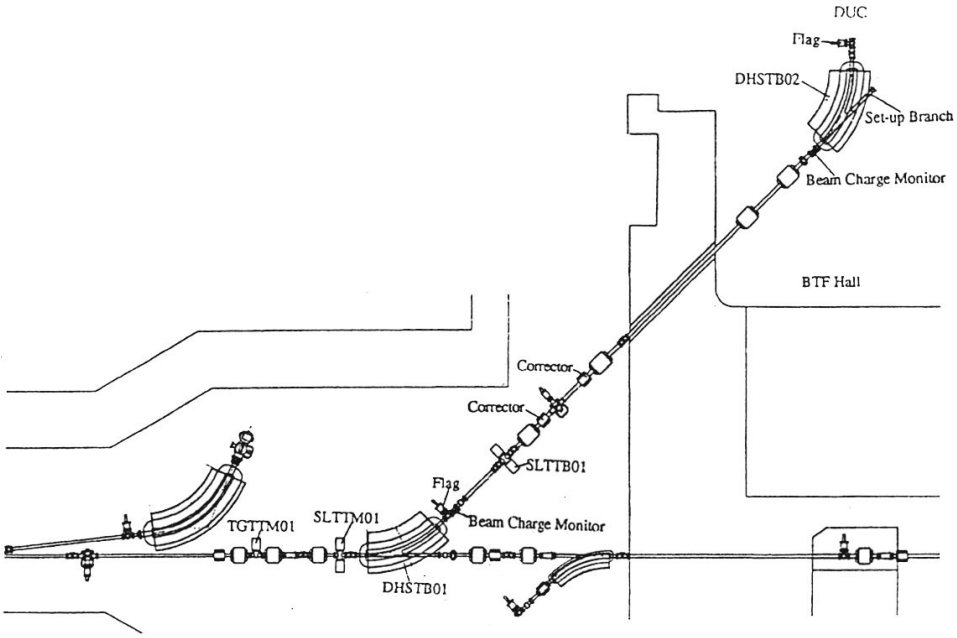

Figure 15: *Layout of the DAΦNE-Linac transfer line and BTF.*

Table 6: Main characteristics of the DAΦNE BTF electron beam.

Maximum beam energy	800 MeV e^-, 550 MeV e^+
Repetition rate	50 Hz
Pulse duration	10 ns
Maximum current per pulse	250 mA ($\simeq 10^{10}$ particles)

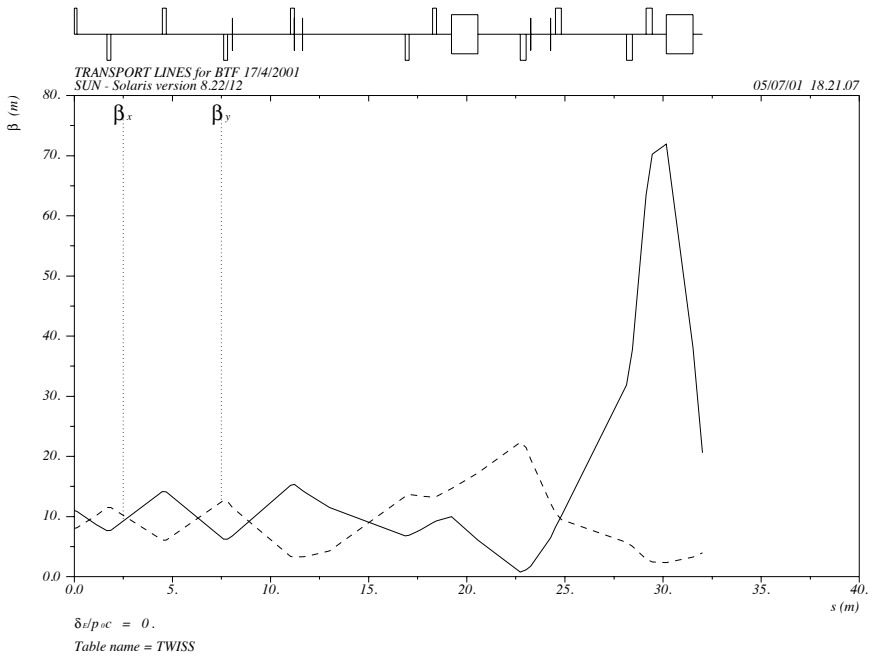

Figure 16: *Calculation of the optical function of the BTF.*

In order to adjust the number of particles in the beam, an energy selection system is used: a moveable target of variable thickness can be inserted in the main Linac line; the beam is then scraped with a slit system before and after entering a bending magnet. Only particles matching the nominal line energy of 510 MeV survive this energy selection (acceptance $\simeq 1\%$). The typical attenuation factor with a two radiation length target is of order 10^7. A fine tuning of the particle number can be performed by modulating the Linac current between the minimum detectable by means of wall current monitors (about 1 mA) and the maximum Linac current. The full range of the BTF beam is then $1 \div 10^{10}$ electrons.

The operating mode for the RAP experiment should be around 10^4 particles per burst (see section 5.7).

5.5 Beam intensity measurement

The measurement of the number of particles in the beam is a crucial point for the evaluation of the effective energy release in the acoustic resonant detector. Moreover, the actual energy deposited should also be monitored, in order to control the "leak" of particles escaping the acoustic detector.

The conventional beam monitors are not effective at low intensities, below 10^6 charged particles, so that particle detectors are necessary. On the other hand, the burst is very short in time ($\simeq 10$ ns), so that a particle detector directly exposed to the beam must be carefully chosen. Moreover,

measurement should be nondestructive, introducing a minimum perturbation to the beam.

A good candidate for such a 'Front detector' could be an ionization chamber: it could be operated in proportional mode in a wide range of gains, according to the beam intensity regime; it is easy to build and operate; it is well known and easy to monitor. Moreover it could provide a direct measurement of the beam intensity once calibrated with an absolute reference. The perturbation to the beam of such a gas detector should be completely negligible. On the other hand, saturation effects have to be carefully controlled: for this purpose the possibility of a secondary emission monitor (SEM) is also under study.

The BTF will be also equipped with a lead/scintillating fiber calorimeter, for general purpose energy, time and multiplicity measurements. This detector was adapted from the "prototype 0" of the KLOE electromagnetic calorimeter. It is made up by two parallelepipeds, made up by 0.5 mm grooved lead foils alternating with cladded 1 mm scintillating fibers (Kuraray SCSF-38 and SCSF-81), glued together, 40 cm length, 14 cm height and 24 cm depth, corresponding to 15 X_0. The readout is via light pipes matching 5 layers of 3.5×3.5 cm^2 portions of the endface to circular photocathodes, plus two bigger cells, 7.0×6.5 cm^2 for a total of $2\times$ 22 channels. Typical measured energy and time resolution for this calorimeter are $5\%/\sqrt{E(\mathrm{GeV})}$ and $70\mathrm{ps}/\sqrt{E(\mathrm{GeV})}$; further details on the characteristics and performances of this detector can be found in [43].

Such a calorimeter could be very useful as 'Back detector' for the RAP experiment in order to monitor the actual energy lost by the particles inside the resonant detector. Even if the resolution for the residual energy measurement downstream of the acoustic detector *on the single electron* is poor, this would be a valuable check for the large anomalous effect that is the objective of the RAP experiment for a shot of $10^3 \div 10^4$ particles (see sec. 5.7).

5.6 Analytical Estimation of the expected signal

In order to compare the signal expected due to particle interaction with the sensitivity of the bar, we can express, according to eq. (2), the signal in Kelvin units. Assuming a bar made of Al5056 ($\rho = 2700\mathrm{kg/m}^3$, $v = 5400\mathrm{m/s}$, $\gamma = 1.6$ [8]) with length of 58.5 cm, the relation for the fundamental mode is the following:

$$T_{signal} = 1.42 \times 10^{-14} \left(\frac{dW}{dx}\right)^2 F_1 \quad Kelvin$$

Neglecting the form factor F_1, that is $\simeq 1$ for impinging particles perpendicular to the longitudinal bar axis, and assuming that all the energy is released

along a path equal to the diameter of the bar (20.5 cm that is about 2.3 X_0), the previous relation can be approximated as follows:

$$T_{signal} \simeq 3.36 \times 10^{-13} \times N_e^2 \times \left(\frac{\Delta W_e}{MeV}\right)^2$$

where N_e is the number of particles impinging the bar, and ΔW_e is the energy released by a single particle.

In our estimation we assume the DAΦNE nominal energy of 510 MeV higher than the critical energy of aluminum (about 60 MeV) so that the dominant energy loss process is the electromagnetic shower. The idea is to modulate the number of electrons impinging on the apparatus in order to release energy inside the bar and excite a detectable mechanical oscillation. From the Monte Carlo simulation (see next section) we know that the average energy released by an electron of 510 MeV is $\simeq$ 224.3 MeV, so that the signal due to a beam of N_e electrons is:

$$T_{signal} \simeq 1.67 \times 10^{-8} N_e^2$$

Assuming a reasonable noise bar temperature of 0.5 Kelvin, the signal due to the impinging particles is:

$$SNR = \left(\frac{T_{signal}}{T_{eff}}\right) = \left(\frac{1.67 \times 10^{-8} N_e^2}{0.5}\right)$$

From this simple evaluation we can estimate that a signal to noise ratio greater than 100 can be achieved using a beam of about 5.5×10^4 electrons. We are working on a full Monte Carlo simulation (described in the next section) in order to evaluate all possible fluctuations and uncertanties, due to energy leakage, beam stability, and thermo acoustic relation uncertainty.

5.7 Monte Carlo simulation

In order to design the experimental setup, to understand the perturbation of the beam due to the cryostat, and the effectiveness of the calorimeter energy measurement, we developed a Monte Carlo simulation based on GEANT 3.21/13 [44]. Another important point is to evaluate the possibility to install the experiment at some distance from the beam line output, in order not to move the setup during other activities at the BTF; in this case the degradation of the beam due to the air layer is to be evaluated.

In the first version of the Monte Carlo program a 510 MeV electron beam with a reasonable emittance, 10^5 m rad^{-1}, 1% of energy spread and 1 cm of transverse dimensions, is impinged on the resonant detector (bar) enclosed in the cryostat after travelling 1.5 m of air. The bar is a 10.25 cm radius, 58.5 cm long Aluminum cylinder, while the cryostat consists of

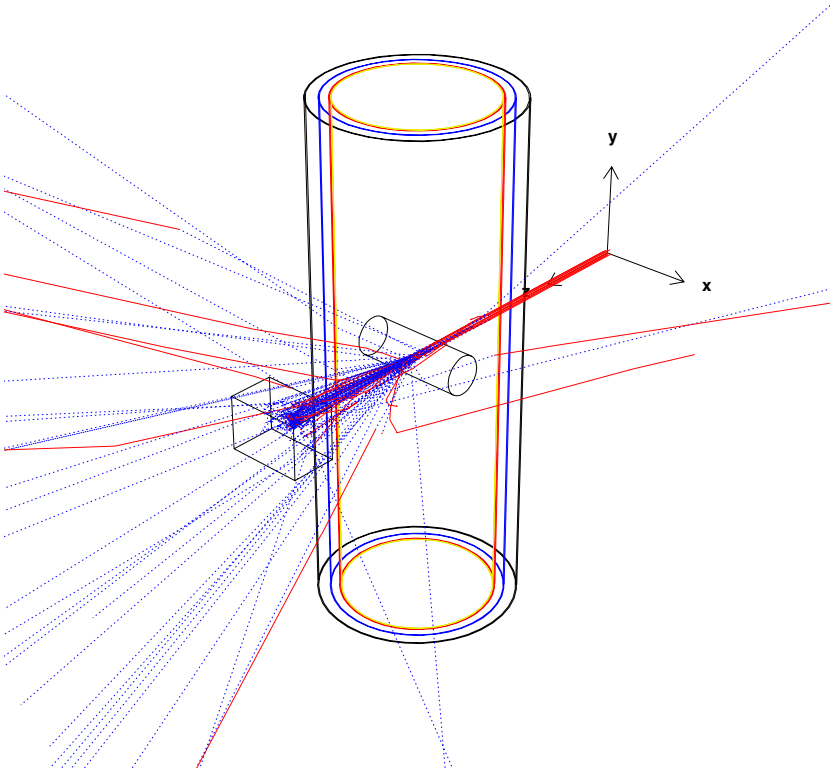

Figure 17: *Example of simulated Monte Carlo events.*

four concentric aluminum shields of 1, 5, 5, and 6 mm thickness. The inner cryostat radius is 39 cm.

The response of the lead/scintillating fibers calorimeter described in the previous sections is also simulated; the real lead/scintillating fibers geometry is replaced by alternating layers of lead and scintillator with an equivalent radiation length and energetic resolution (see details in [45]).

An example of simulated events is shown in fig. 17 with the back detector placed at 20 cm from the cryostat.

The effect on the beam spread due to the cryostat and the air for a 10^4 electrons shot is shown in fig. 18: the low energy tail is mainly due to soft photons irradiated when crossing the thin aluminum shields.

The energy loss in the bar can be used to evaluate the response in terms of temperature increase in the acoustic detector.

The energy deposited in the resonant detector can also be correlated with the response of the calorimeter. As shown in fig. 19, with 10^3 e^- shots accuracy on the energy release in the bar of the order of 3% can be achieved (for an ideal calorimeter, the real performances taking into account photoelectron statistics should be better than 5%).

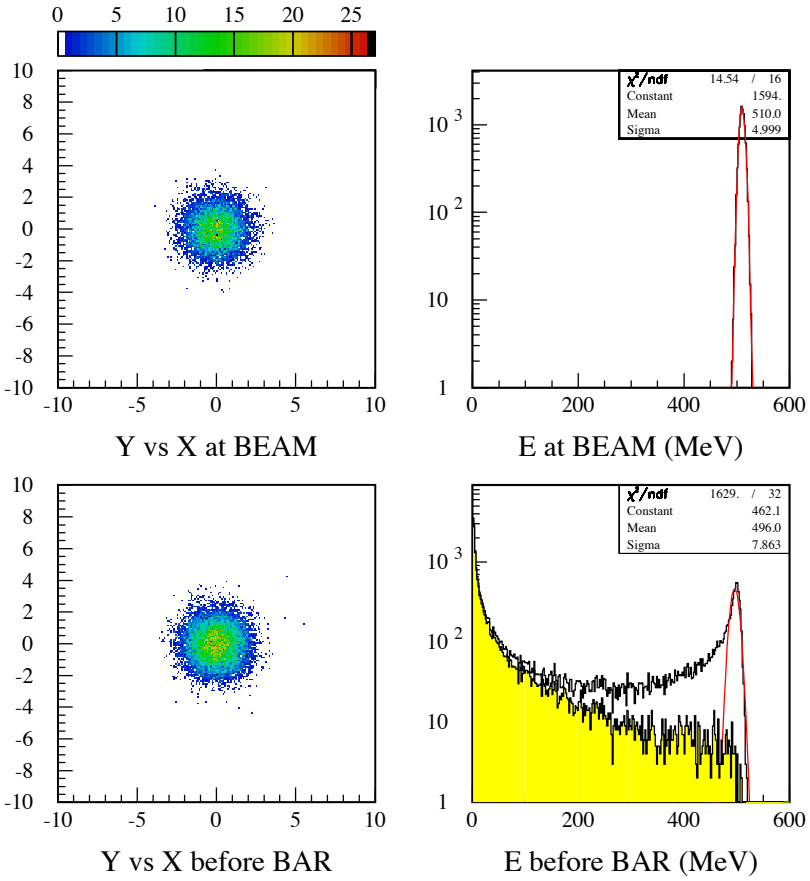

Figure 18: *Beam spread due to cryostat (before entering the resonant detector): transverse plane distribution and energy distribution before (up) and after (down) crossing the cryostat walls; the shaded distribution refers to photons.*

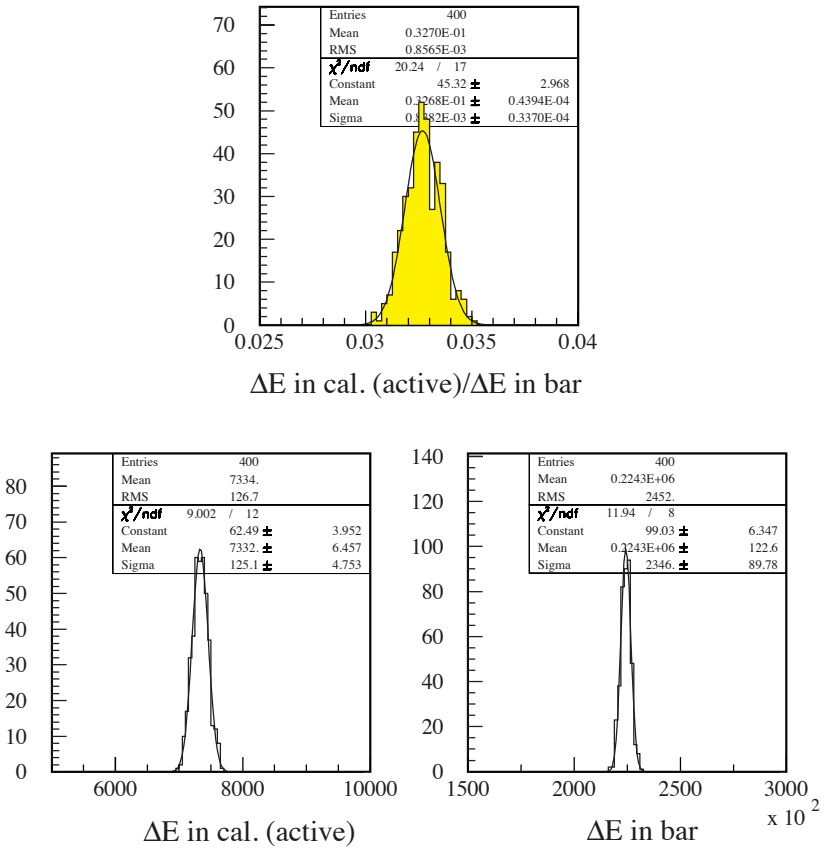

Figure 19: *Energy release in the bar, the active material and in the whole calorimeter (MeV) for 400 runs of 10^3 e^- impinging on the apparatus.*

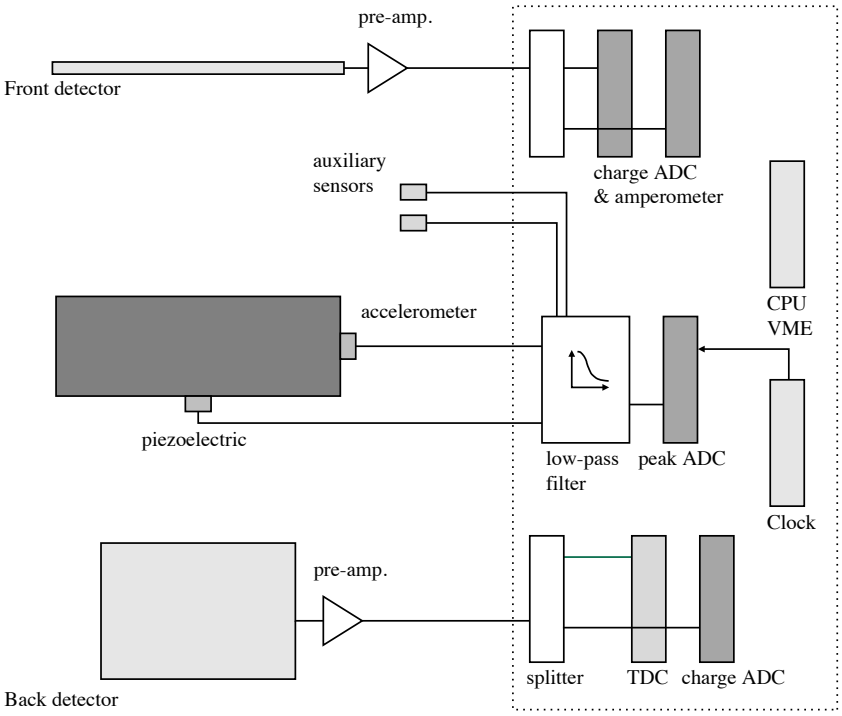

Figure 20: *Schematic layout of the DAQ chain.*

5.8 Data acquisition

The acquisition should collect data from the various parts of the experiment (as shown in fig. 20) both from the acoustic detector and from the beam intensity monitors:

- the piezoelectric and the accelerometer signals from the acoustic detector;
- the beam monitor before hitting the resonant detector (Front detector);
- the beam energy measurement from the calorimeter downstream of the acoustic detector (Back detector);
- some auxiliary sensors, like thermometer, seismic sensors, etc., to monitor all the experimental conditions.

Concerning the resonant detector, the data acquisition is intended to

- measure the Brownian motion and electrical noise of the mechanical resonant detector;

- measure the resonance amplitude due to the energy loss by particles hitting the detector;
- measure the anomalous amplitude (large energy events);

These characteristics translate into the requirement for the DAQ system of good accuracy and sensitivity over a wide range of event amplitudes. Moreover, the system must also have a good sampling accuracy in order to avoid spurious signal reconstruction (such as aliasing).

In order to use well known and common-use standards at DAΦNE experiments, we plan to use an VME-based acquisition system [46]:

- VMEbus single-board computer **VMIC** VMIVME 7751 with Linux operating system;
- VME peak sensing ADC, CAEN, 12 bit range;
- custom KLOE splitter board [43];
- VME charge ADC and TDC for the KLOE calorimeter, CAEN, 12 bit range (see [43]);
- TDC.

6 Summary and requests

6.1 RAP detector main parameters

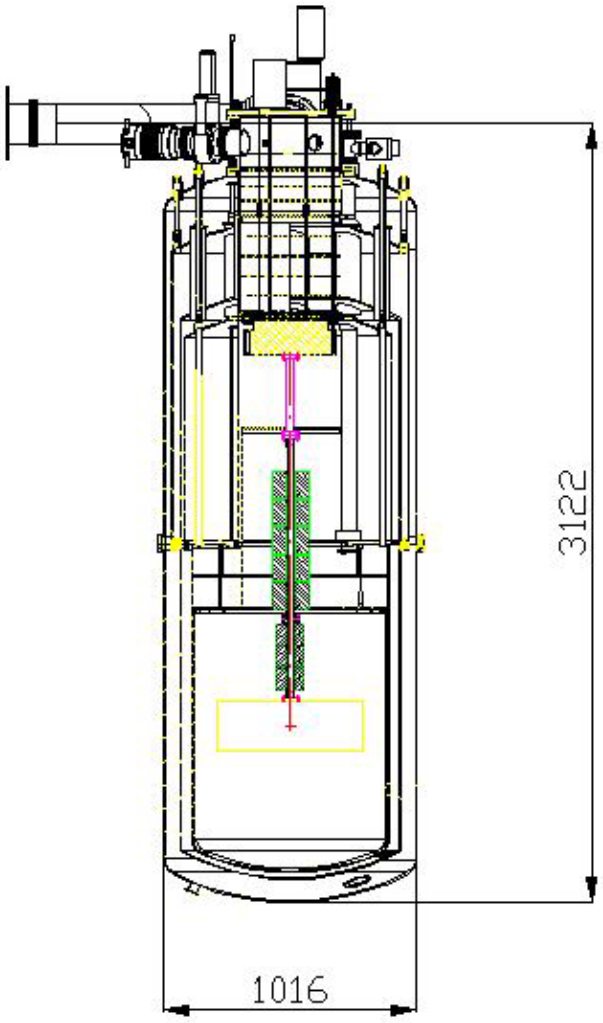

Figure 21: *Schematic layout of the apparatus.*

Table 7: RAP detector main parameters

test mass	Al5056 cylinder; lenght = 585 mm, diameter = 205 mm, M = 52 kg, resonance frequency $\simeq$ 4.6 kHz
cryostat	commercial aluminum cryostat; height = 3200 mm, diameter = 1016 mm
^{3}He $-^4$ He dilution refrigerator	base temperature = 100 mK, cooling power at 120 mK = 1 mW
suspension	multistage stainless steel-copper suspension system; overall attenuation around 4 kHz $\simeq -150$ dB
read-out	piezoelectric ceramics + FET amplifier with calibration capabilities
beam	500 MeV energy e^-, pulsed/single shot operation mode maximum current per pulse = 250 mA
acquisition	VME based on-line acquisition samplig rate = 100 kHz

6.2 The Collaboration

Implementation of the experiment requires the construction of the detector and its installation at the DAΦNE BTF at LNF.

The institutions involved in the experiment are LNF, Roma Tor Vergata, Leiden and Barcelona. LNF and Roma are involved in the aspects related to the set-up of the experiment and data analysis. The Leiden group is involved in the cryogenics and Barcelona in the theoretical and phenomenological aspects of the project, as well as in data analysis.

The Leiden and Barcelona group will use TARI European funds for travel and data taking.

6.3 Costs of the experiment

The main costs of the experiment are: dilution refrigerator (45 kEuro), vacuum pumps (40 kEuro), suspensions and apparatus assembly (20 kEuro), data acquisition (10 kEuro), sensors and electronics (9 kEuro).

The cost due to specific requirements for the beam of the experiment will be covered by the DAΦNE operation group. A cryostat borrowed from the ROG group will be used.

The overall cost of the project is 147 kEuro, mainly concentrated in the first year of the experiment implementation.

6.4 Time schedule

We plan to conclude this research in three years, starting from the approval, according to the following milestones:

$T_{approval}$ + 12 months	Construction and first measurements
$T_{approval}$ + 24 months	Data taking with the DAΦNE BTF facility
$T_{approval}$ + 36 months	Data analysis and, if necessary, further data taking with the beam

References

[1] ROG collaboration, P. Astone *et al.*, Astropart. Phys. **7**, 231 (1997).

[2] ROG collaboration, P. Astone *et al.*, Phys. Rev. Lett. **84**, 14 (2000).

[3] B.L. Beron, R. Hofstander, Phys. Rev. Lett. **23**, 184 (1969).

[4] B.L. Beron, S.P. Boughn, W.O. Hamilton, R. Hofstander, T.W. Tartin, IEEE Trans. Nucl. Sci. **17**, 65 (1970).

[5] A.M. Grassi Strini, G. Strini, G. Tagliaferri, J. Appl. Phys. **51**, 849 (1980).

[6] A.M. Allega, N. Cabibbo, Lett. Nuovo Cimento **83**, 263 (1983).

[7] C. Bernard, A. De Rujula, B. Lautrup, Nucl. Phys. B **242**, 93 (1984).

[8] A. De Rujula, S.L. Glashow, Nature **312**, 734 (1984).

[9] E. Amaldi, G. Pizzella, Nuovo Cimento **9**, 612 (1986).

[10] B. Liu, G. Barish, Phys. Rev. Lett. **61**, 271 (1988).

[11] G.D. van Albada *et al.*, Rev Sci Instrum. **71**, 1345 (2000).

[12] E. Coccia, A. Marini, G Mazzitelli, G. Modestino, F. Ricci, F. Ronga, L. Votano, Nucl. Instrum. Methods Phys. Res., Sect. A **335**, 624 (1995).

[13] ROG collaboration, P. Astone *et al.*, Phys. Lett. B **499**, 16-22 (2001).

[14] L. Sulak *et al.*, Nucl.Inst. Meth. **161**, 203 (1979).

[15] G. Bressi *et al.*, *Consuntivo degli esperimenti PPCS e PICI INFN-Gruppo V*, unpublished.

[16] G. Carugno *et al.*, Europhys.Lett, **24**, 713 (1993);
F. Bordoni *et al.*, in *Experimental Gravitation*, Institute of Physics Publishing, **A285** (1993).

[17] G. Cocconi, *Encyclopedia of Physics*, ed. by S. Flugge **46** 1, 228 (1961).

[18] D. Heck *et al.*, Report FZKA 6019, Forschungszentrum Karlsruhe (1998).

[19] J.R Horandel *et al.*, ICRC Cosmic Ray Conference, Salt Lake City **1**, 337 (1999).

[20] E. Witten, Phys. Rev. D **30**, 272 (1984).

[21] ROG collaboration, P. Astone *et al.*, Physical Review D **47** 10, 4770 (1993).

[22] S. Coleman, Nucl. Phys. B **262** (1985).

[23] E.R. Fitzgerald, Nature **252**, 638 (1974).

[24] P. G. de Gennes, *Superconductivity of Metals and Alloys*, Benjamin, New York (1966).
T. Van Duzer, and C. W. Turner, *Principles of Superconductive Devices and Circuits*, Prentice Hall (1998).

[25] A. Barone, *Superconductive Particle Detectors*, World Scientific, Singapore (1988).

[26] *Low Temperature Detectors for Neutrinos and Dark Matter*, ed. by K. Pretzl, N. Schmitz, L. Stodolsky, Springer, Berlin (1987).

[27] R.F. O'Connell, Phys. Lett. A **282**, 257 (2001).

[28] G.W. Ford, J.T. Lewis, R.F. O'Connell, Phys. Rev. A **37**, 4419 (1988).

[29] G.W. Ford, J.T. Lewis, R.F. O'Connell, Phys. Rev. Lett. **55**, 2273 (1985).

[30] G. Frossati, E. Coccia, Cryogenics **35**, 9 (1994).

[31] A.D.Cimpoiasu, *The suspension of the GRAIL gravitational wave antenna*, (P.H.D. Thesis).

[32] B.Aalami, B.Atzori, *Flexural vibrations and Timoshenko beam theory*, AIAA Journal **12**, 5 (1974).

[33] Nabarro Editor, *Dislocations in Solids*, (volume 6).

[34] M.Beccaria et al., *The creep problem in the VIRGO suspensions: a possible solution using Maraging steel*, Nucl. Instrum. Methods Phys. Res. A **404**, 455-469 (1988).

[35] G.Cagnoli et al, *Mechanical shot noise induced by creep in suspension devices*, Phys. Lett. A **237**, 21-27 (1997).

[36] J.K.Tien, C.T.Yen, *Cryogenic creep of metals*, Henry Crumb School of Mines, Columbia University.

[37] R.P Giffard, Phys. Rev. D **14**, 2478 (1976).

[38] G.V. Pallottino, G. Pizzella, Nuovo Cimento C **4**, 237, (1981).

[39] H.J. Paik, *Electromechanical transducers and bandwidth for resonant-mass detectors*, ed. by E. Coccia, G. Pizzella, F. Ronga, Proceedings of the First Edoardo Amaldi Conference on Gravitational Wave Experiments, 201-219, World Scientific (1995).

[40] U. Giovanardi, G.V. Pallottino, *Metodi di calibrazione di un'antenna gravitazionale*, (CNR, Laboratorio di Ricerca e Tecnologia per lo Studio del Plasma nello Spazio Italy, 1977), Rep. no. LPS-77-6.

[41] A. Ghigo and F. Sannibale, *Single Electron Operation Mode in DAΦNE BTF*, Proceedings of the Fourth European Particle Accelerator Conference, World Scientific (1994).

[42] F. Sannibale and G. Vignola, *DAΦNE-Linac Test Beam*, DAΦNE Technical Note **LC-2** (1991).

[43] The KLOE Collaboration, *The KLOE Electromagnetic Calorimeter*, LNF-01/017 (P), (2001).

[44] CERN ASG, *Detector description and simulation tool*, CERN Program Library W5013.

[45] A. Parri, *A simulation of the prototype of the KLOE e.m. calorimeter*, KLOE Note xx (199x);
S. Bertolucci, S. Miscetti, *Results on energy and time response and resolution for the barrel EMCAL prototype*, KLOE Note 45 (1992).

[46] G. Mazzitelli, *VME-Real-Time Data Acquisition for the Ultracryogenic Gravitational Antenna of Third Generation*, LNF-96/024 (IR), (1996).